

NASA TECHNICAL NOTE



NASA TN D-7087

NASA TN D-7087

WIND-TUNNEL MEASUREMENTS OF
SURFACE-PRESSURE FLUCTUATIONS AT
MACH NUMBERS OF 1.6, 2.0, AND 2.5
USING 12 DIFFERENT TRANSDUCERS

by

Thomas L. Lewis
Flight Research Center
Edwards, Calif. 93523

and

Jules B. Dods, Jr.
Ames Research Center
Moffett Field, Calif. 94035

1. Report No. NASA TN D-7087		2. Government Accession No.		3. Recipient's Catalog No.	
4. Title and Subtitle WIND-TUNNEL MEASUREMENTS OF SURFACE-PRESSURE FLUCTUATIONS AT MACH NUMBERS OF 1.6, 2.0, AND 2.5 USING 12 DIFFERENT TRANSDUCERS				5. Report Date October 1972	
				6. Performing Organization Code	
7. Author(s) Thomas L. Lewis (Flight Research Center), and Jules B. Dods, Jr. (Ames Research Center)				8. Performing Organization Report No. H-700	
9. Performing Organization Name and Address NASA Flight Research Center P. O. Box 273 Edwards, California 93523				10. Work Unit No. 501-24-12-00-24	
				11. Contract or Grant No.	
12. Sponsoring Agency Name and Address National Aeronautics and Space Administration Washington, D. C. 20546				13. Type of Report and Period Covered Technical Note	
				14. Sponsoring Agency Code	
15. Supplementary Notes					
16. Abstract <p>The turbulent boundary layer on the wall of a 9- by 7-foot wind tunnel was measured with 12 different transducers at Mach numbers of 1.6, 2.0, and 2.5. The results indicated that the wall surface-pressure-fluctuation field was more homogeneous at a Mach number of 2.5 than at Mach numbers of 1.6 or 2.0. A comparison of power-spectral-density data at Mach 2.5 with a summary of similar data (Mach 0.1 to 3.45) showed good agreement.</p> <p>The measurement uncertainty was greatest when frequencies were low and the surface-pressure-fluctuation field was homogeneous. The uncertainty at higher frequencies increased as the surface-pressure-fluctuation field became more nonhomogeneous. Since transducer mounting effects and system noise levels were determined not to have contributed appreciably to measurement uncertainties, the result was attributed to an interaction between the surface-pressure-fluctuation field and the transducers.</p> <p>Corcos' correction for size effects improved the comparison between transducers at the high frequencies, but did not eliminate an apparent size effect at the lower frequencies. Thus absolute values of the power spectral density of surface-pressure fluctuations should be interpreted with caution. This result suggests that methods of reducing the effect of the presence of the transducer, such as the "pinhole" transducer technique, should be studied.</p>					
17. Key Words (Suggested by Author(s)) Transducer response Aerodynamic noise			18. Distribution Statement Unclassified - Unlimited		
19. Security Classif. (of this report) Unclassified		20. Security Classif. (of this page) Unclassified		21. No. of Pages 49	22. Price* \$3.00

WIND-TUNNEL MEASUREMENTS OF SURFACE-PRESSURE FLUCTUATIONS AT MACH NUMBERS OF 1.6, 2.0, AND 2.5 USING 12 DIFFERENT TRANSDUCERS

Thomas L. Lewis
Flight Research Center

and Jules B. Dods, Jr.
Ames Research Center

INTRODUCTION

Measurement of surface-pressure fluctuations is an important source of information about the nature of the dynamic environment of aircraft and space shuttle vehicles. It is important that this environment be well defined so that proper laboratory testing can be utilized to insure structural integrity of these vehicles. There has, however, been considerable doubt among experimenters about the accuracy of the data obtained in supersonic boundary layers. This concern led to the present investigation.

Twelve different types of transducers were used to make comparative measurements of supersonic boundary layers on a wind-tunnel wall. The transducers were selected on the basis of availability and previous use by other experimenters. Measurements were made simultaneously with 11 of these transducers in an array on the side wall of the NASA Ames Research Center 9- by 7-foot supersonic wind tunnel. Eleven transducers of the twelfth type were placed in another identical array to obtain measurements for use as reference data. The reference transducer array was used to define the surface-pressure-fluctuation field and to correct for position location so that data from the different transducers could be compared directly.

All the transducers were calibrated on the tunnel wall. Altitude sensitivity, low-frequency rolloff, resonance effects, and Corcos (ref. 1) spatial size effect corrections were made during data analysis.

This investigation determined differences in the surface-pressure-fluctuation measurements made by the 12 different types of transducers. The differences were considered to constitute the measurement uncertainty. This uncertainty is expressed in this report in terms of percentage deviation about a mean value of the spread in the data. Selected data are compared with a summary of the data compiled by Bies in reference 2.

SYMBOLS

Physical quantities in this report are given in the International System of Units and parenthetically in U. S. Customary Units. Calculations and measurements were made in U. S. Customary Units. Factors relating the two systems are presented in reference 3.

C	nondimensional frequency used to obtain the Corcos correction, $\omega r/0.7U$
C_f	skin-friction coefficient
F	nondimensional frequency, $\log_{10}\left(\frac{f}{f_{\text{ref}}}\right)$
f	frequency, Hz
f_{ref}	reference frequency, 20 Hz
h_p	pressure altitude, m (ft)
l	arbitrary reference length, 0.0254 m (0.083 ft)
M	free-stream Mach number
\hat{P}	nondimensional estimated power spectral density, $\log_{10}\left[\frac{\overline{P^2(f)U}}{q^2 l} \times 10^7\right]$
\hat{P}'	nondimensional estimated power spectral density from reference 2, $\log_{10}\left[\frac{\overline{P^2(\omega)U}}{\tau_w^2 \delta^*} \times 10^3\right]$
\hat{P}_c	Corcos correction to the estimated power spectral density
$\overline{P^2(f)}$	power spectral density as a function of frequency, $\frac{(\text{hN/m}^2)^2}{\text{Hz}} \quad (\frac{\text{lbf/ft}^2)^2}{\text{Hz}})$
$\overline{P^2(\omega)}$	power spectral density as a function of circular frequency, $(\text{hN/m}^2)^2 \text{sec} \quad ((\text{lbf/ft}^2)^2 \text{sec})$
q	free-stream dynamic pressure, hN/m^2 (lbf/ft^2)
R	Reynolds number per unit length, m^{-1} (ft^{-1})
r	radius of the transducer diaphragm, cm (in.)
SPL	sound pressure level, dB
T_t	total temperature, °K (°R)
U	free-stream velocity, m/sec (ft/sec)

U_c	convection velocity, m/sec (ft/sec)
V	nondimensional voltage, $\log_{10} (\text{volts} \times 10^5)$
x_t	distance to the tunnel throat, m (ft)
δ	boundary-layer height, m (ft)
δ^*	boundary-layer-displacement thickness, m (ft)
Θ	boundary-layer-momentum thickness, m (ft)
Λ	nondimensional frequency from reference 1, $\log_{10} \left(\frac{\omega \delta^*}{U} \times 10^4 \right)$
λ	wave length of a surface-pressure fluctuation, m (ft)
τ_w	skin friction, hN/m^2 (lbf/ft^2)
ψ	nondimensional frequency, $\log_{10} \left(\frac{f l}{U} \times 10^4 \right)$
ω	circular frequency, rad/sec

TEST APPARATUS

Test Fixture

The transducer test fixture, shown in figure 1, was designed as a sealed unit to insure that the wind-tunnel static pressure existed on both sides of the transducers. (The importance of maintaining a zero differential pressure across the transducer diaphragm was shown during a previous attempt to obtain data using one of the transducers.) The chamber portion and the rear plate of the fixture were fabricated from 0.635-centimeter (0.25-inch) brass stock, and the transducer mounting plate, 15.2 centimeters (6 inches) in diameter, was machined from a 2.54-centimeter (1-inch) piece of brass stock. O-rings were used to obtain a pressure seal between the chamber and the front and rear plates. The assembled unit was tested in a laboratory vacuum chamber to insure that the seal was airtight. The static pressures within the test fixture and the wind tunnel were also monitored during the test to make sure that they remained the same.

Comparison Transducer Plate

Figure 2(a) shows the arrangement of the 11 different transducers in the comparison transducer plate. Pertinent information about the transducers is given in table 1. Additional information may be obtained from the manufacturers and from reference 4 for the WEAL transducer. An estimate of the sensitive diameter of each transducer

was determined solely by measuring either the movable portion of the diaphragm or the exposed portion of the crystal. A more detailed analysis of the effective sensitive diameter is presented in reference 5 for the condenser transducers and in reference 6 for the piezoelectric transducers. The estimated sensitive diameters used in this test are believed to yield corrected values of estimated power spectral density, \hat{P} , which are within 0.1 of values determined by using the more detailed analyses.

Reference Transducer Plate

Figure 2(b) shows the arrangement of the reference (Kulite) transducers in the reference transducer plate. This mounting plate is of the same design as the comparison transducer plate of the test fixture; however, the sealed circular chamber was not needed because only a small-diameter venting tube was necessary to obtain equal static pressure across the diaphragms.

TEST FACILITY

The experiment was conducted in the Ames Research Center 9- by 7-foot supersonic wind tunnel. This facility is a closed-circuit, continuous-flow wind tunnel which is capable of producing constant Mach number flows from 1.55 to 2.5. Mach number can be varied by moving the fixed-contour block that forms the floor of the nozzle. This facility is described in detail in reference 7.

TEST PROCEDURE

The face of the transducer mounting plate was installed flush with the inside wall of the wind tunnel. Figure 3 shows the approximate location of the transducer group in the wind-tunnel test section. Shown on the sting body is a model from which data were taken on alternating runs as part of a separate study. Its position was believed to be remote enough not to affect the present test.

Before the tests were started, the following laboratory calibrations were made on each transducer: voltage sensitivity, electrostatic, acoustic pressure coupler, and free field response. The results of these calibrations are shown in figures 4 to 15.

The transducers were then mounted in the transducer fixture shown in figure 1. The technique used to insure that the tolerance for mounting flushness was held within 0.0000 and -0.0025 centimeter (0.000 and -0.001 inch) is illustrated in figure 16. These tolerances were considered to be critical in the effort to eliminate avoidable sources of error. An accelerometer was also mounted on the back of the comparison plate to measure the vibrational environment of the transducers. The sensitive axis of the accelerometer was perpendicular to the plane of the sensitive surfaces of the transducers. After the transducers were installed, the transducer fixture was mounted to the side wall of the tunnel, using the same tolerances for flushness.

The transducers were tested while they were installed in the tunnel wall. The

electrostatic calibrator shown in figure 17, which was developed at the NASA Flight Research Center, was used to insure that the transducers would function properly under the reduced ambient pressures encountered in the test. The calibrator was held in position over the transducers by a vacuum holding chamber (inset, fig. 17). The pressure in the chamber housing the electrostatic actuator was reduced to levels corresponding to the pressure altitudes of the test. At each pressure altitude, the voltage output from each transducer caused by a constant 1000-hertz input was recorded. The basic electrostatic calibration technique is explained in detail in reference 8.

Test data were obtained for wind-tunnel operating Mach numbers of 1.6, 2.0, and 2.5. The resulting tunnel flow parameters of interest for these tests for each Mach number are presented in table 2. During the tests the data were recorded on magnetic tape. The recorder was operated at 1.52 meters per second (60 inches per second), and frequency modulation was used to record data over a frequency range from 0 to 20,000 hertz.

The transducer fixture was then rotated 180° so that the downstream transducers became upstream transducers, and the three test conditions were rerun to eliminate possible upstream transducer effects on the former downstream transducers.

Finally, the comparison transducer plate was replaced by the reference transducer plate and the tests were repeated. No Kulite transducer was installed in the comparison plate because previous tests using Kulite transducers in this wind tunnel had shown that the estimated power spectral density of the pressure fluctuation did not vary more than 0.1 over all frequencies for repeated tunnel test conditions.

A pressure calibration signal was recorded on tape just prior to each test; this signal was used to establish the gain of the system for data reduction. A hybrid computer system developed by the NASA Ames Research Center (ref. 9) was used to obtain the power spectral densities with and without the Corcos correction. The data were then corrected by using laboratory calibrations.

DATA CORRECTION PROCEDURE

The results of the laboratory calibrations from which corrections for sensitivity and frequency response were determined are presented in figures 4 to 15. Low-frequency rolloff was corrected by the use of the acoustic pressure coupler frequency response.

Altitude sensitivity corrections for eight of the transducers were obtained by means of an electrostatic calibration. This technique was not adaptable to the WEAL, AR, Kistler, and Kulite transducers. The altitude sensitivity of the WEAL transducer was determined through acoustic coupler responses (fig. 5). No altitude sensitivity corrections were considered necessary for the AR, Kistler, and Kulite transducers.

Corrections needed for resonance effects were determined from the electrostatic response of the transducers (figs. 4 to 15). The effects of resonance are shown at values of F near 3 and vary from a slight upward reflex to a well-defined resonant peak. The Photocon 514 transducer required the largest correction for resonance and size. The

results of these corrections are shown in figure 18. The amplitude of the response for frequencies affected by resonance can be shown from calibration data to be a linear function of pressure altitude, so that linear extrapolation can be used to determine resonance for off-calibration data points. Because the frequency of the resonance and the damping characteristics for a gridded transducer, for example, Photocon 504 and ES, change somewhat with the introduction of a flow field, the correction becomes uncertain. This may also be true for nongridded transducers; however, the correction shown in figure 18 appears to be of the right order.

The Corcos method of correction for the spatial size of the transducer (ref. 1) is presented in a more convenient form in figure 19. The value of \hat{P}_C for the frequency for which a correction is desired is added to \hat{P} at that frequency. This correction affects noticeably only that portion of the spectrum for which $\psi > 3$.

The system noise of each transducer was recorded and reduced to power-spectral-density format for each of the three test conditions. These system noise spectra were then compared with the raw data spectra, and with the aid of figure 20 (standard method of correcting noise levels based upon power equations) the corrections due to system noise were made for the frequencies affected.

ACCURACY

The tolerances for flushness in mounting the transducers were considered to be very important. Reference 10 shows the importance of achieving good transducer flushness to minimize what is referred to as the self-noise effect. Coe (ref. 11) shows the effect of nonflushness on the measurement of surface-pressure fluctuations; his work led to the flushness tolerances used in this test. The tolerances were checked before and after the test runs with the dial indicator system illustrated in figure 16.

On the basis of the three types of frequency-response calibrations performed on each transducer, the corrected data were estimated to be accurate to within ± 5 percent, that is, ± 0.5 dB. The accuracy of the power spectral densities was not measurably affected by wind-tunnel wall vibrations. The highest vibration level in any one frequency determined by spectral analysis was 0.016g, which was too low to cause any significant voltage output from the transducers.

On the basis of repeated laboratory tests, the accuracy of the three types of frequency response calibrations performed on each transducer was estimated to be within ± 5 percent (that is, ± 0.5 dB).

The data were reduced by using a hybrid computer system (ref. 9). The statistical accuracy of the system varied somewhat with frequency, as indicated by the normalized standard error in table 3 (from ref. 12). The normalized standard error, which is presented in terms of percent, is defined as follows:

$$\text{Normalized standard error} = \frac{\sqrt{\frac{\text{Variance of the sample mean value}}{\text{True mean square value}}}}{\times 100 \text{ (ref. 13)}}$$

According to Bendat (ref. 13) the normalized standard error can be determined by using

the following expression:

$$\frac{1}{\sqrt{(\text{Filter bandwidth})(\text{Averaging time})}}$$

RESULTS AND DISCUSSION

The values of the parameters used in this analysis of surface-pressure-fluctuation data are given in table 2 for each of the three test conditions. The boundary-layer parameters were determined in a previous test in which a 25.4-centimeter (10-inch) boundary-layer rake was positioned 46.2 centimeters (18.25 inches) downstream of the transducer location. These boundary-layer parameters were adjusted to the location of the transducers.

The spectra measured by the reference Kulite transducers, corrected for size, are plotted in figure 21 for each test condition. This figure shows the upper and lower boundaries of the data spread as well as the mean. At a Mach number of 1.6, the data show a variation in estimated power spectral density of approximately 0.8, corresponding to a variation of ± 45 percent about the mean pressure level for almost two orders of magnitude in frequency (that is, for $\psi = 1$ to 3). At $M = 2.0$, the largest variation in \bar{P} is approximately 0.6, which represents a variation of ± 35 percent (at $\psi \approx 1.5$). The variation in the spectra for the test at a Mach number of 2.5 is approximately ± 15 percent over the entire frequency range analyzed (10 to 20,000 hertz).

These data are an indication of the nature of the pressure-fluctuation field for each of the test conditions. If the power spectral density of the pressure-fluctuation field is invariant as measured by the transducer array, the pressure-fluctuation field may be considered to be homogeneous. The test condition for a Mach number of 2.5 can therefore be considered to have the most nearly homogeneous pressure-fluctuation field. The data for Mach numbers of 2.0 and 1.6 show progressively larger degrees of non-homogeneity in the pressure-fluctuation field. The reason for these larger variations is not known; however, the variations may be associated with the distance of the test location from the tunnel throat. This distance, as shown in table 2, was longest for the test at a Mach number of 2.5 and shortest for the test at a Mach number of 1.6. Longer flow length may have allowed the pressure-fluctuation field to become more homogeneous.

Although the flow conditions at Mach numbers of 1.6 and 2.0 cannot be considered representative of homogeneous surface-pressure fluctuation, they do represent conditions for which a determination of measurement accuracy is needed.

Figures 22 to 24 present the data from all the transducers. The data from each transducer are presented according to location and are compared with the data from the corresponding reference transducer (the Kulite transducer in the same position). The short-dashed lines represent the raw data, and the solid lines represent the corrected measurements of surface-pressure-fluctuation power spectral density.

As these figures show, there are some large differences between the raw data and the corrected values of the estimated power spectral density. The WEAL transducer shows the largest differences over the greatest frequency range (figs. 22(b), 23(b), and 24(b)). This is attributed primarily to the need for altitude sensitivity correction, as

shown in figure 5(c). Because of the system noise interference in the laboratory, the correction for the lower frequencies is not known. The largest corrections for low-frequency rolloff were made to data from the B & K transducer (figs. 22(g), 23(g), and 24(g)). This correction was determined from the response of the acoustic pressure coupler presented in figure 10(c). Data from the Photocon 514 transducer were corrected for the largest resonant effect (figs. 23(i) and 24(i)). Corrections for resonance were based on the results of the electrostatic calibrator response (fig. 12(b)). Although this correction is approximate, a brief comparison with the results from transducers not requiring this correction shows it to be of the right magnitude.

Effect of Transducer Size

The data obtained with the Photocon transducers vary with transducer size, as illustrated in figure 25. These data were corrected for position location by determining the difference in estimated power spectral density, as a function of frequency, between the reference transducer at each location and the reference transducer at location 1. The result was then algebraically added to the data from each of the comparison transducers.

Although the Corcos correction was also added to the data, transducer size still seems to affect the measurement. This is most apparent in figure 25(a), where the amplitude of the measured spectra is inversely proportional to the diaphragm diameter over most of the frequency range. The data in figures 25(b) and 25(c) show the same trend, except for the data of the 0.483-centimeter (0.19-inch) Photocon transducer, which tends to yield lower values in the lower frequencies. It is also apparent, again with the exception of this transducer, that the different transducers yielded data in especially good agreement in the Mach 2.5 test when the pressure-fluctuation field was apparently more nearly homogeneous. The agreement is especially significant because of the large differences in transducer size (from 0.305 centimeter to 0.991 centimeter (0.12 inch to 0.39 inch)).

Similar size effects are not as evident in figure 26 for different manufacturers' transducers. The shaded areas represent the spread of the Photocon transducer data (figs. 25(a) to 25(c)). The measurements of the 0.508-centimeter (0.2-inch) LTV transducer are, in general, higher than those of the 0.406-centimeter (0.16-inch) B & K transducer; however, the data of the larger (0.711-centimeter (0.28-inch)) WEAL transducer are in general lower, except at a Mach number of 2.5.

Data from the piezoelectric transducers are compared in figure 27. In general, even though the Corcos correction had been applied, the smallest transducers again yielded the largest values. The exception was the Kistler transducer, which read low at Mach 1.6 but high at Mach 2.5 for low frequencies. Because system noise was in general somewhat higher at these low frequencies for this transducer, the possibility that it had influenced the data was investigated. However, system noise was found to have negligible effect.

Surface Interaction

Bhat (The Boeing Co.) and Hanly and Dods (NASA Ames Research Center) found in separate unpublished experiments that transducers that protruded yielded higher

power-spectral-density levels than those that were flush with the surface. Some of the work by Hanly and Dods, reported in reference 11, indicated that the amount of the increase was proportional to the free-stream dynamic pressure and to the ratio of the protrusion height to the laminar sublayer thickness. The level of power spectral density increased in all frequencies, with the lower frequencies affected most. Although a similar trend toward higher levels of power spectral density can be seen in the data presented here, particularly in the lower frequencies, the mounting tolerances of all transducers were held rigidly within 0.0000 and -0.0025 centimeter (0.000 and -0.001 inch). The tolerances were also checked before and after the test runs. Despite these precautions, the power-spectral-density measurements differed. These differences may have been caused by an interaction between the surface of the transducer and the turbulent flow, as discussed in the next paragraph.

The largest difference in measurement for the homogeneous pressure fluctuation field (Mach 2.5) appeared in the lowest frequencies. (As shown in figure 21(c), the reference (Kulite) transducer measured nearly the same values over the entire frequency range.) This would seem to imply that the greatest uncertainty in measurement is in the measurement of the largest wavelengths. However, as indicated by Wills (ref. 14), the frequency bandpass filters used to determine these power spectral densities cannot distinguish between surface-pressure fluctuations of large wavelengths that move quickly and small wavelengths that move slowly. If the wavelength of a surface-pressure fluctuation is determined from both its frequency and its convection velocity, as indicated by $\lambda = U_c/f$, and if it is assumed that the convection velocity of the lowest frequency is about 0.8U, at Mach 2.5 the wavelength would be 47.5 meters (156 feet). If low-frequency measurements correspond to large wavelength phenomena, a small transducer mounted with the exacting tolerances of this test should have little, if any, effect on the measurements, because all the transducers would measure the same value of a purely acoustic pressure fluctuation at these frequencies. However, the variation in amplitude of the lowest frequencies is large, which could be explained if the wavelengths related to these frequencies are small. This would indicate that the origin of the pressure fluctuation is near the surface of the wall. Similar interpretations have been made by other experimenters. Blake, in reference 15, showed data which indicate that the convection velocity decreases in the lower frequencies. Bhat (ref. 16) concluded that uncertainties in the lowest frequencies were associated with an eruption of disturbances from very close to the wall. Thus the large variation in these data may be due to an interaction between the surface-pressure-fluctuation field and the transducer.

Data Summary

Figures 25 to 27 show large differences in the data from the 11 different transducers over most of the frequency range analyzed. These data are summarized in figure 28 (all data are corrected to location 1). The Mach 1.6 test condition (fig. 28(a)) shows the greatest uncertainty over the largest frequency range. The uncertainty is as great as ± 75 percent (1.6P) for $\psi \approx 2$.

The data for Mach 2.0 (fig. 28(b)) show an uncertainty of ± 55 percent (1.0P) for $\psi \approx 2$; however, the uncertainty for $\psi \approx 0.7$ increases to ± 80 percent (1.7P).

Although the reference transducer shows an uncertainty of approximately ± 15 percent over the analyzed range for the Mach 2.5 test condition, the results from the

comparative test group indicate the greatest uncertainty of the test at this condition. At $\psi \approx 0.5$, the uncertainty is ± 85 percent ($2.2\hat{P}$); however, for $\psi > 2.5$, the uncertainty decreases to approximately ± 15 percent ($0.3\hat{P}$).

Because the frequencies of greatest uncertainty (that is, $\psi \leq 2$) are frequencies to which the Corcos finite size correction does not apply, there is a large degree of uncertainty in comparing data from different transducers.

Because of this difficulty in obtaining similar measurements with dissimilar transducers, it seems appropriate to suggest that transducers be standardized; however, no transducer showed clear superiority in this test. The test results do indicate an interaction between the surface-pressure-fluctuation field and the transducer, and that this interaction influences a larger portion of the frequency range as the surface-pressure-fluctuation field becomes more nonhomogeneous.

A possible alternative to standardization would be to reduce or eliminate transducer interaction with the flow. One method might be to recess the transducer below the surface and use a small hole in the surface (pinhole) as a path for the pressure fluctuations to reach the transducer.

Because of the nonhomogeneous nature of the surface-pressure-fluctuation field in the turbulent boundary layer at Mach 1.6 and 2.0, only the data at Mach 2.5 can be compared with measurements made by other experimenters. The largest scatter in the Mach 2.5 test is of about the same order as that in the Bies summary (fig. 29).

The Mach 2.5 data are compared with a data summary plot by Bies (ref. 2) in figure 29. (The ordinate and the abscissa in this figure are not in the same form as in figure 28.) The data have been nondimensionalized by using the skin-friction coefficient and circular frequency (the form used by Bies). The agreement between these measurements and those taken during other wind-tunnel experiments is reasonably good. Bies does not present data for values of ψ less than approximately 2.5.

CONCLUDING REMARKS

Twelve different types of transducers were used to measure the surface-pressure fluctuations on the wall of the NASA Ames Research Center 9- by 7-foot wind tunnel. Data were obtained at Mach numbers of 1.6, 2.0, and 2.5. The results indicated that the wall surface-pressure-fluctuation field is more homogeneous at a Mach number of 2.5 than at Mach numbers of 1.6 or 2.0. A comparison of power-spectral-density data at Mach 2.5 with a summary of similar data (Mach 0.1 to 3.45) showed good agreement.

The measurement uncertainty was greatest when frequencies were low and the surface-pressure-fluctuation field was homogeneous. The uncertainty at higher frequencies increased as the surface-pressure-fluctuation field became more nonhomogeneous. Since transducer mounting effects and system noise levels were determined not to have contributed appreciably to measurement uncertainties, the result was attributed to an interaction between the surface-pressure-fluctuation field and the transducers.

Although the Corcos finite size correction appeared to be of the right magnitude at higher frequencies, it did not eliminate the size effects that seemed to dominate the lower frequency portion of the spectrum. These effects became apparent when the data from transducers of different sizes were compared. In general, the small-diameter transducers yielded higher power-spectral-density values in all frequencies than the larger-diameter transducers.

Available laboratory calibration techniques could not correct for interaction between the surface-pressure-fluctuation field and the transducer. It is believed that this interaction was the major cause of measurement uncertainty. Thus absolute values of the power spectral density of surface-pressure fluctuations should be interpreted with caution.

Because it is so difficult to obtain similar measurements with dissimilar transducers, standardization of transducers would seem to be appropriate; however, no transducer showed a clear superiority in this investigation. The test results do indicate, however, that an interaction between the surface-pressure-fluctuation field and the transducer causes large uncertainties in the data. Thus a possible alternative to transducer standardization to reduce this interaction could be the "pinhole" transducer technique.

Flight Research Center

National Aeronautics and Space Administration

Edwards, Calif., April 21, 1972.

REFERENCES

1. Corcos, G. M.: Resolution of Pressure in Turbulence. *Acoustical Soc. Am.*, vol. 35, no. 2, Feb. 1963, pp. 192-199.
2. Bies, D. A.: A Review of Flight and Wind Tunnel Measurements of Boundary Layer Pressure Fluctuations and Induced Structural Response. Bolt Beranek and Newman Inc. (NASA CR-626), 1966.
3. Mechty, E. A.: The International System of Units - Physical Constants and Conversion Factors. NASA SP-7012, 1969.
4. Ortega, J. C.: Microphone System for the Measurement of Boundary Layer Pressure Fluctuations. Tech. Rep. AFFDL-TR-66-196, Air Force Flight Dynamics Lab., Wright-Patterson Air Force Base, Jan. 1967.
5. Murphy, J. S.; Bies, D. A.; Speaker, W. V.; and Franken, P. A.: Wind Tunnel Investigation of Turbulent Boundary Layer Noise as Related to Design Criteria for High Performance Vehicles. NASA TN D-2247, 1964.
6. Schloemer, H. H.; and Recine, E. C.: Effects of a Sudden Change in Surface Roughness on Turbulent Boundary-Layer Wall-Pressure Fluctuations. *U. S. Navy Underwater Acoustics*, vol. 20, no. 2, Apr. 1970, pp. 305-314.
7. Staff of the Ames Research Center: Research Facilities Summary. Vol. II-Wind Tunnels. Subsonic, Transonic and Supersonic. NASA, Dec. 1965.
8. Anon.: Brüel & Kjaer Technical Review, No. 1. B & K Instruments, Inc., 1965, p. 11.
9. Lim, R. S.; and Cameron, W. D.: Power and Cross-Power Spectrum Analysis by Hybrid Computers. NASA TM X-1324, 1966.
10. Richards, E. J.; and Mead, D. J.: Noise and Acoustic Fatigue in Aeronautics. Ch. 8, M. K. Bull, John Wiley & Sons, Ltd., 1968, p. 179.
11. Coe, C. F.: Surface-Pressure Fluctuations Associated With Aerodynamic Noise. Basic Aerodynamic Noise Research, NASA SP-207, 1969, pp. 409-424.
12. Chyu, W. J.; and Hanly, R. D.: Power- and Cross-Spectra and Space-Time Correlations of Surface Fluctuating Pressures at Mach Numbers Between 1.6 and 2.5. NASA TN D-5440, 1969.
13. Bendat, J. S.; and Piersol, A. G.: Measurement and Analysis of Random Data. John Wiley & Sons, Inc., c.1966, p. 186.
14. Wills, J. A. B.: Measurements of the Wave-Number/Phase Velocity Spectrum of Wall Pressure Beneath a Turbulent Boundary Layer. *J. Fluid Mech.*, vol. 45, part 1, Jan. 1970, pp. 65-90.

15. Blake, W. K. : Turbulent Boundary-Layer Wall-Pressure Fluctuations on Smooth and Rough Walls. J. Fluid Mech., vol. 44, part 4, Dec. 1970, pp. 637-660.
16. Bhat, W. V. : Flight Test Measurement of Exterior Turbulent Boundary Layer Pressure Fluctuations on Boeing Model 737 Airplane. J. Sound and Vibration, vol. 14, no. 4, Feb. 1971, pp. 439-457.

TABLE 1. - TRANSDUCER INFORMATION

Location	Transducer	Transducer type	Sensitivity, dB (ref. 1 volt/N/m ²)	Estimated sensitive diameter, cm (in.)	Manufacturer
Reference	Kulite	Diffusion-bonded, semi-conductor, strain-gage pressure transducer, model XPL-125-4HF	-63	0.102 (0.04)	Kulite Semiconductor Products, Inc.
1	Photocon	Condenser microphone, model 734	-50	.305 (.12)	Whittaker Corp.
2	IWEAL	Condenser microphone, model A-6	-60	.711 (.28)	Western Electric-Acoustic Lab., Inc.
3	LTV	Condenser microphone, model HF-CF-1	-56	.508 (.20)	Ling-Temco-Vought Research Center
4	AR	Lead-zirconate-titanate piezoelectric pressure transducer, model LD-107	-83	.305 (.12)	Atlantic Research Corp.
5	BBN	Lead-zirconate (G-1500) piezoelectric acoustic sensor, model 376A	-65	.508 (.20)	Bolt Beranek and Newman, Inc.
6	ES	Lead-titanate-zirconate piezoelectric transducer, model 299507 (gridded)	-55 (-35)	.711 (.28)	Gulton Industries
7	B & K	Condenser microphone, model 4136	-63	.406 (.16)	Brüel & Kjaer
8	Photocon	Grid-covered condenser microphone, model 504	-40	.940 (.37)	Whittaker Corp.
9	Photocon	Condenser microphone, model 514	-42	.991 (.39)	Whittaker Corp.
10	Photocon	Condenser microphone, model 614	-52	.483 (.19)	Whittaker Corp.
11	Kistler	Quartz pressure transducer, model 6061.	-62	.610 (.24)	Kistler Instrument Corp.

¹This microphone is scaled, whereas the other condenser microphones are vented.

TABLE 2. -- TEST CONDITIONS

	M		
	1.6	2.0	2.5
U, m/sec (ft/sec)	468 (1537)	536 (1760)	595 (1951)
q, hN/m ² (lbf/ft ²)	427 (892)	362 (756)	260 (542)
R, m ⁻¹ (ft ⁻¹)	13.2×10^6 (4.01×10^6)	11.4×10^6 (3.46×10^6)	9.09×10^6 (2.77×10^6)
x _t , m (ft)	7.64 (25.07)	9.04 (29.67)	10.67 (35.02)
δ, m (ft)	.118 (.387)	.105 (.344)	.104 (.340)
δ*, m (ft)	.0168 (.0550)	.0186 (.0608)	.0229 (.0750)
Θ, m (ft)	.00765 (.0251)	.0063 (.0206)	.0060 (.0197)
C _f	1.39×10^3	1.32×10^3	1.18×10^3
h _p , m (ft)	10.6×10^3 (34.9×10^3)	14.4×10^3 (47.4×10^3)	19.6×10^3 (64.2×10^3)
T _t , °K (°R)	306 (582)	303 (578)	299 (570)

TABLE 3. - OPERATING PARAMETERS FOR THE HYBRID ANALOG-DIGITAL ANALYSIS OF POWER SPECTRAL DENSITIES

[From ref. 12]

Frequency range, Hz	Filter bandwidth, cycles	Averaging time, sec	Number of filters	Normalized standard error of power spectral densities, percent
10 to 50	2	20	21	15.8
60 to 240	10	20	19	7.0
260 to 1,020	40	10	20	5.0
1,200 to 5,200	200	2	21	5.0
5,600 to 10,400	400	2	13	3.5
11,200 to 20,000	800	2	12	2.5

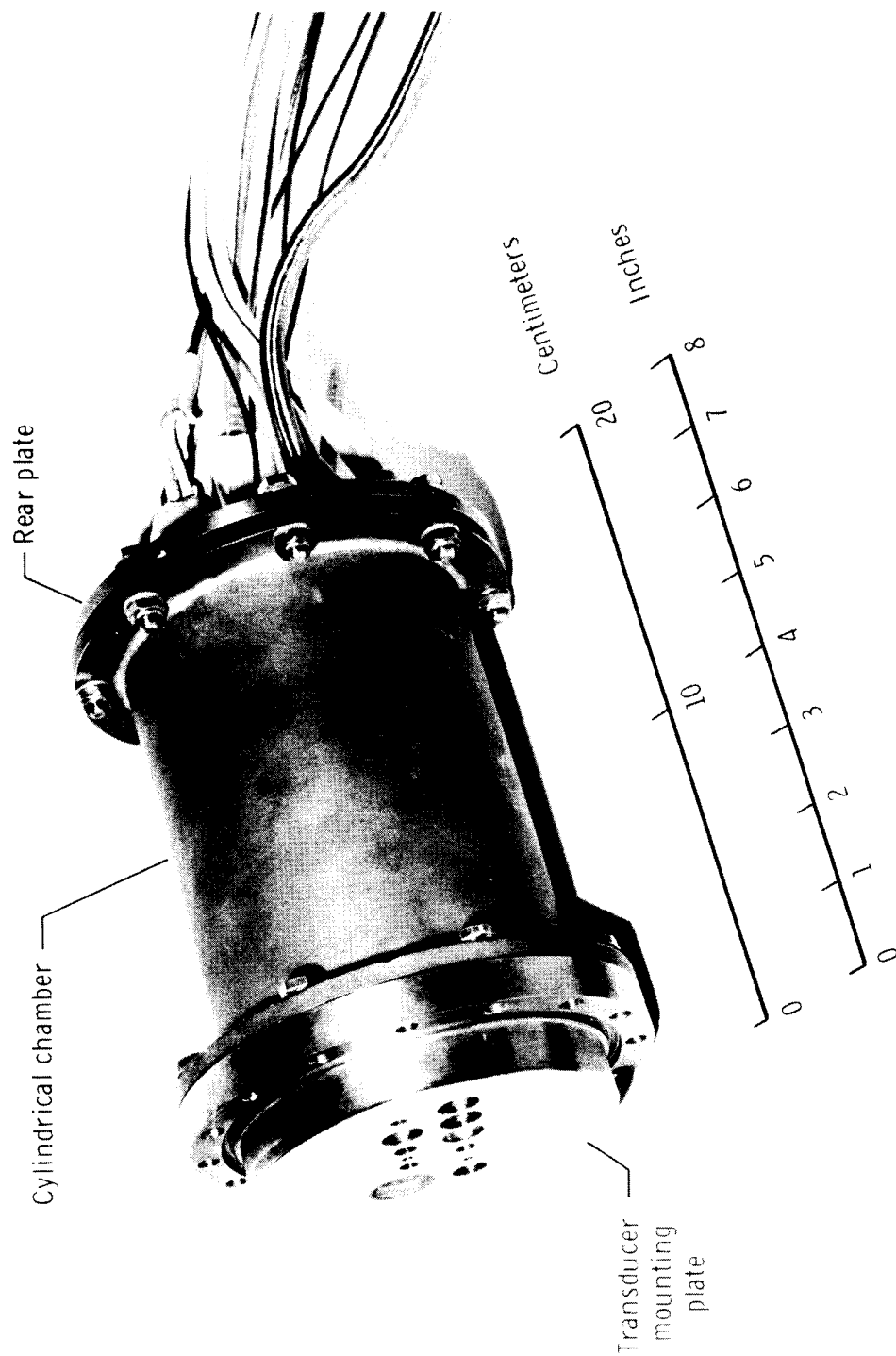
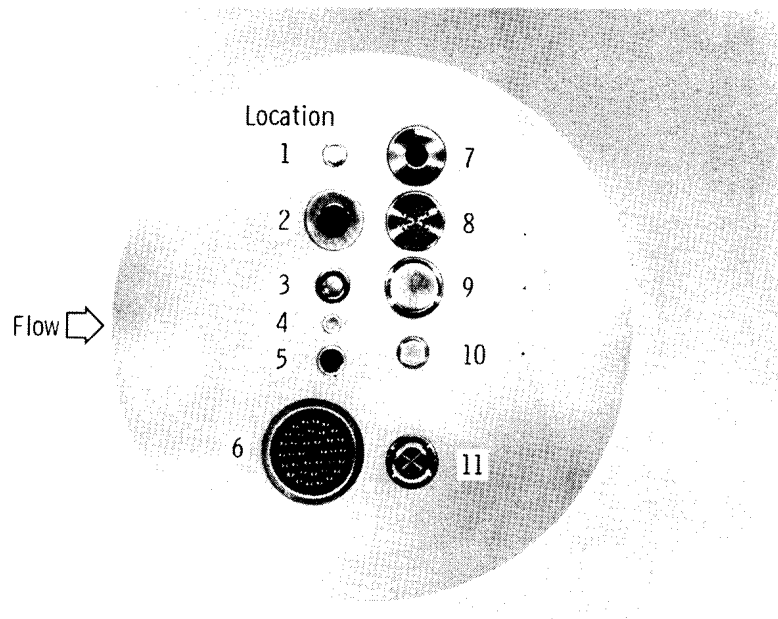
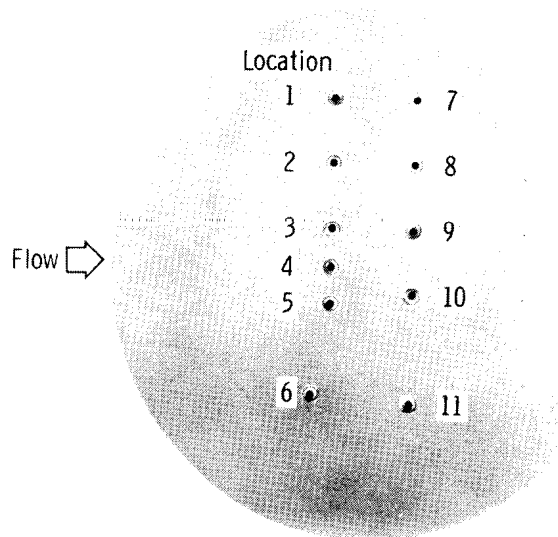


Figure 1. Wind-tunnel wall fixture in which 11 different transducers were installed.



(a) Comparison transducer plate in which 11 different transducers were mounted.



(b) Reference transducer plate in which 11 model XPL-125-4HF Kulite transducers were mounted.

Figure 2. Transducer mounting plates installed in the tunnel wall, showing the locations of the transducers used in the tests. (Plates were rotated 180° for measurements at locations 7 to 11.)

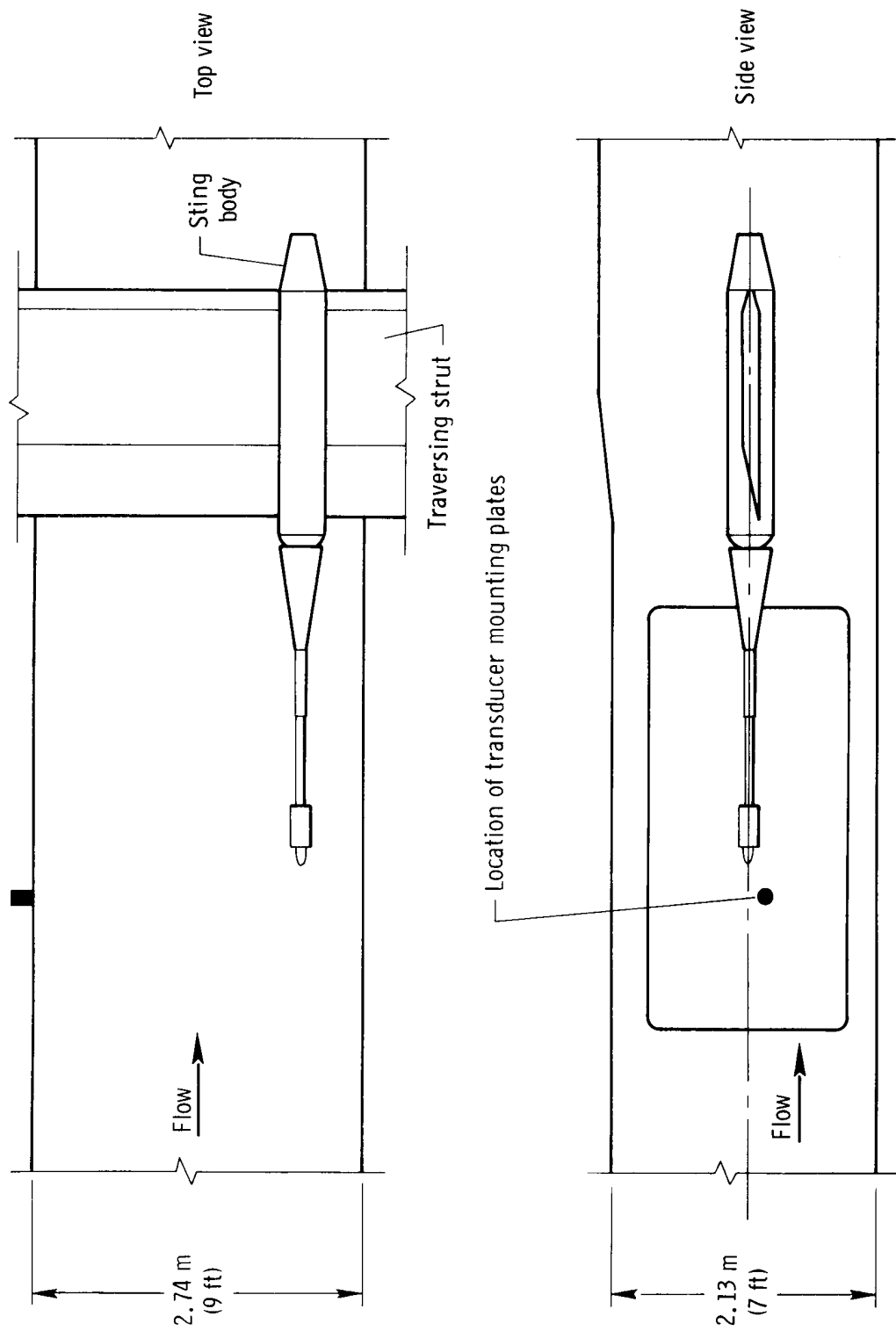
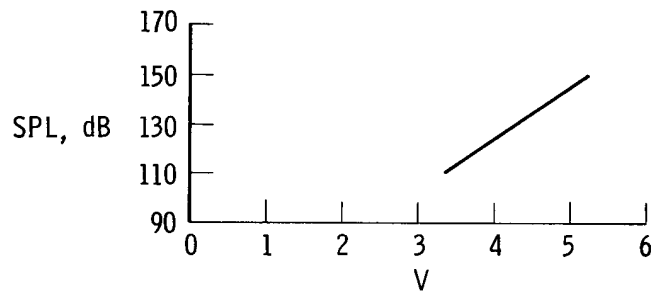
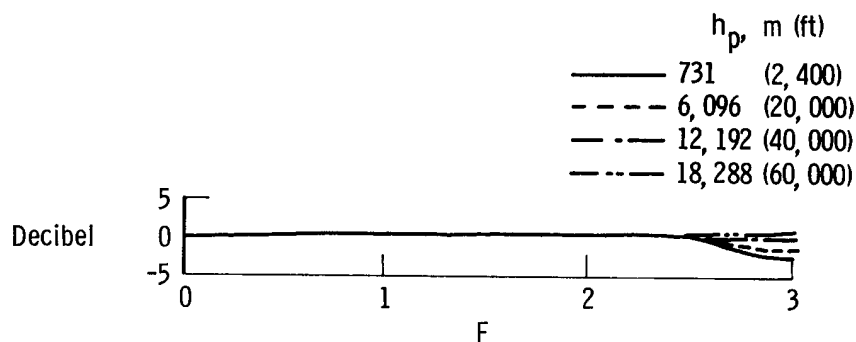


Figure 3. Sketch showing the approximate location of the transducers in the 9 - by 7 -foot wind tunnel.



(a) Transducer sensitivity (-50 dB ref. 1 volt/N/m²).



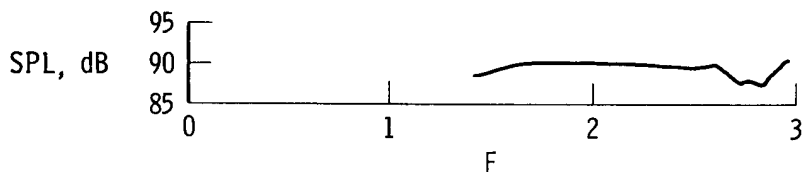
(b) Electrostatic altitude sensitivity response.



(c) Acoustic pressure coupler response.

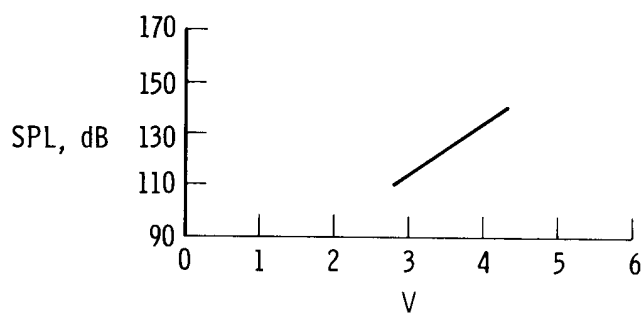


(d) Parallel incidence free field response.

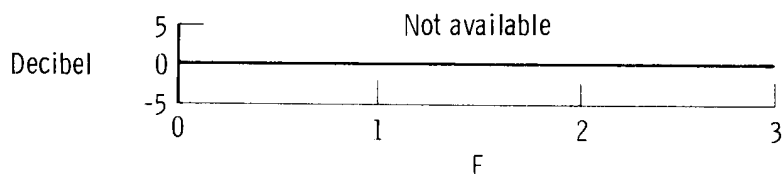


(e) Perpendicular incidence free field response.

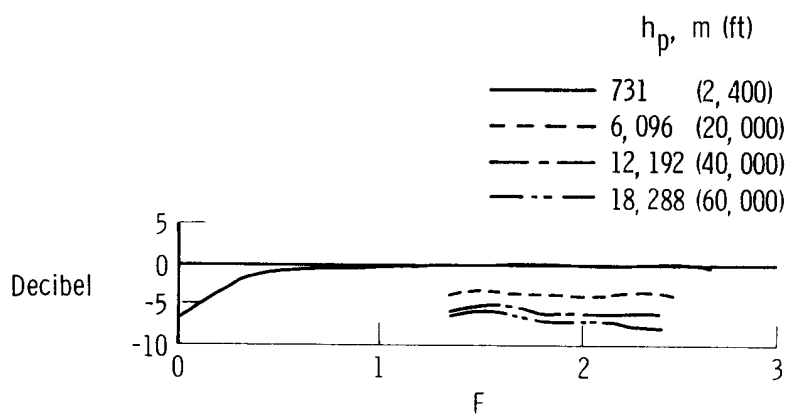
Figure 4. Laboratory calibration for the Photocon model 734 microphone (location 1).



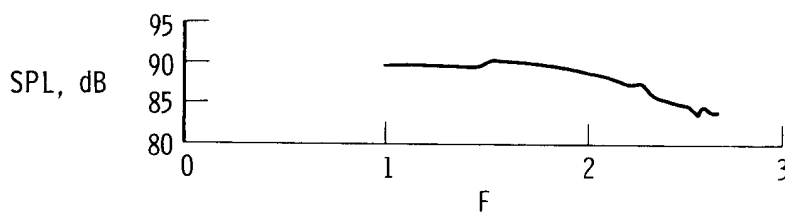
(a) Transducer sensitivity (-60 dB ref. 1 volt/N/m²).



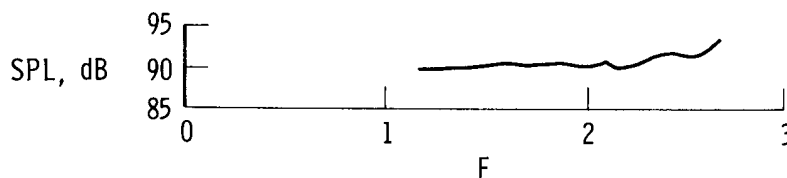
(b) Electrostatic altitude sensitivity response.



(c) Acoustic pressure coupler response.

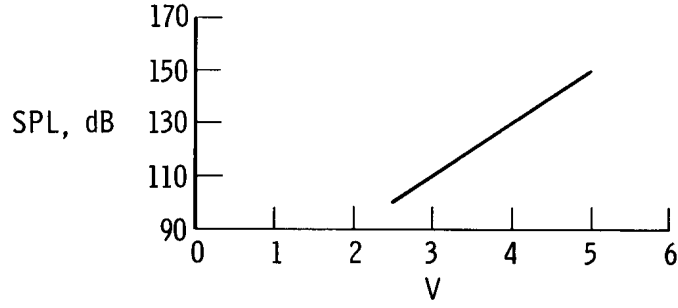


(d) Parallel incidence free field response.

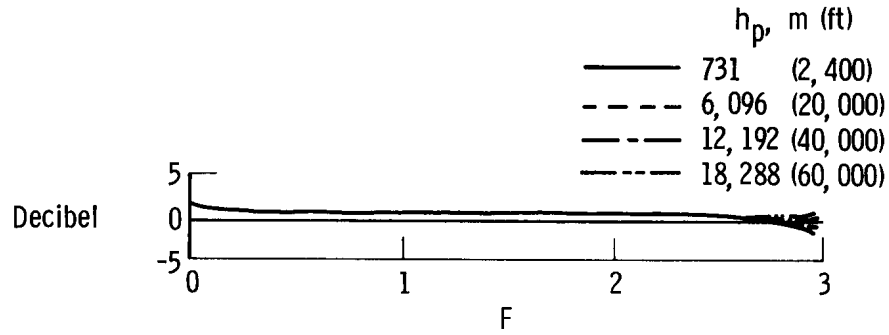


(e) Perpendicular incidence free field response.

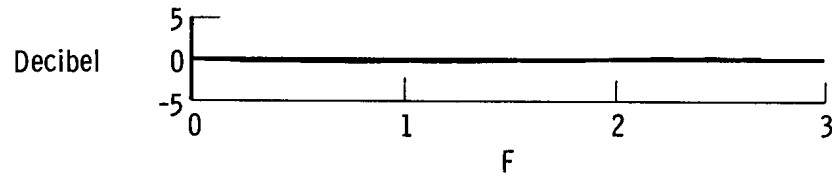
Figure 5. Laboratory calibration for the WEAL model A-6 microphone (location 2).



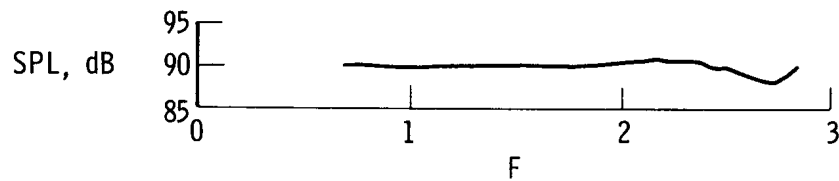
(a) Transducer sensitivity (-56 dB ref. 1 volt/N/m²).



(b) Electrostatic altitude sensitivity response.



(c) Acoustic pressure coupler response.

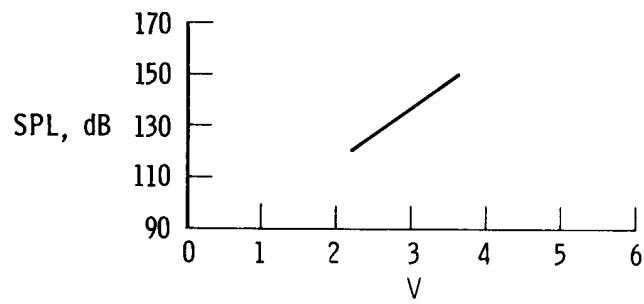


(d) Parallel incidence free field response.

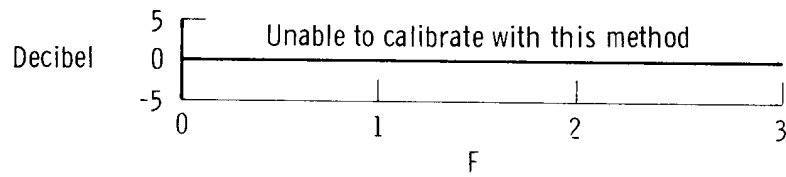


(e) Perpendicular incidence free field response.

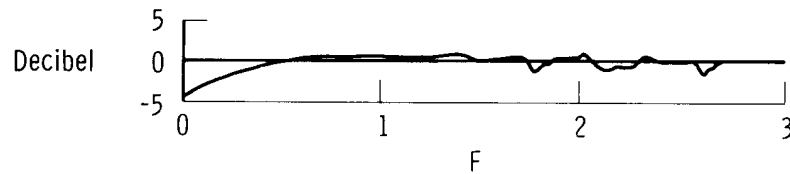
Figure 6. Laboratory calibration for the LTV model HF-CF-1 microphone (location 3).



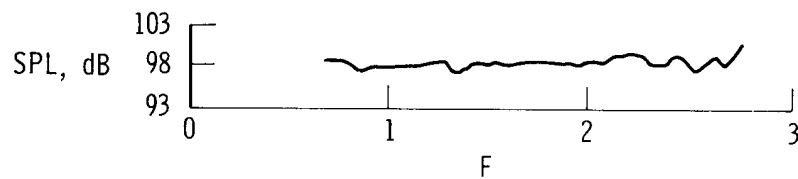
(a) Transducer sensitivity (-83 dB ref. 1 volt/N/m²).



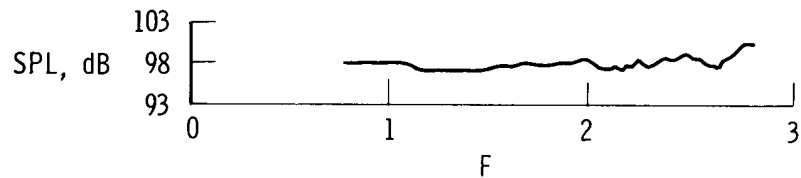
(b) Electrostatic altitude sensitivity response.



(c) Acoustic pressure coupler response.

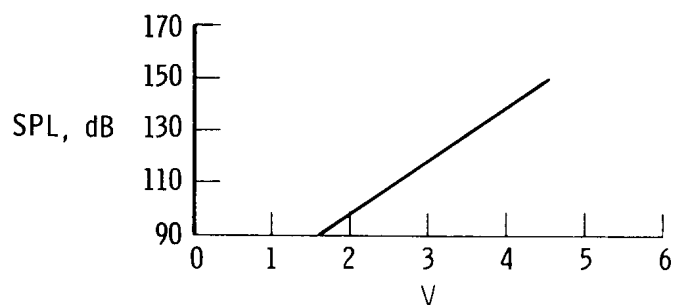


(d) Parallel incidence free field response.

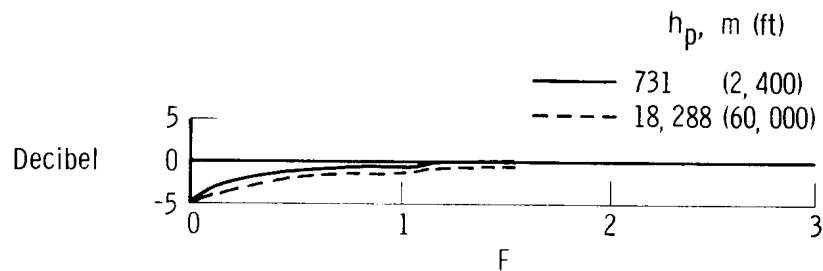


(e) Perpendicular incidence free field response.

Figure 7. Laboratory calibration for the AR model LD-107 microphone (location 4).



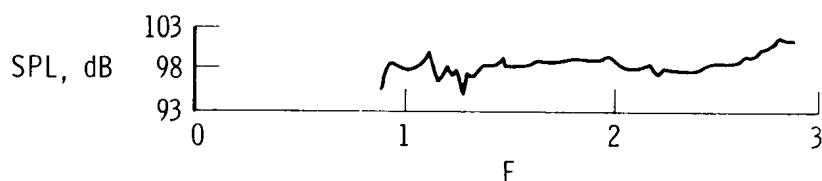
(a) Transducer sensitivity (-65 dB ref. 1 volt/N/m²).



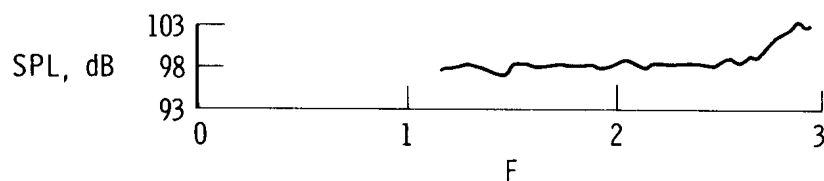
(b) Electrostatic altitude sensitivity response.



(c) Acoustic pressure coupler response.

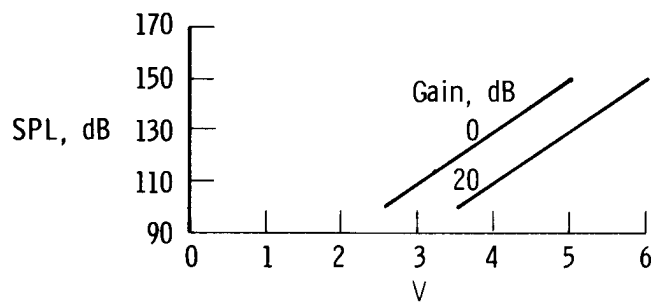


(d) Parallel incidence free field response.

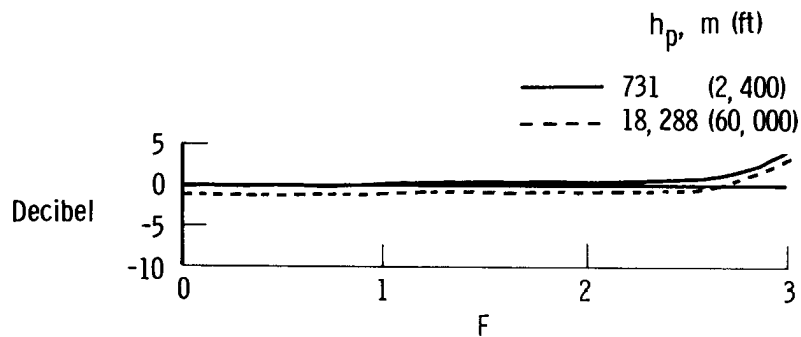


(e) Perpendicular incidence free field response.

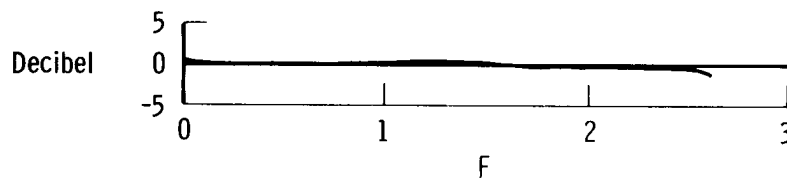
Figure 8. Laboratory calibration for the BBN model 376A microphone (location 5).



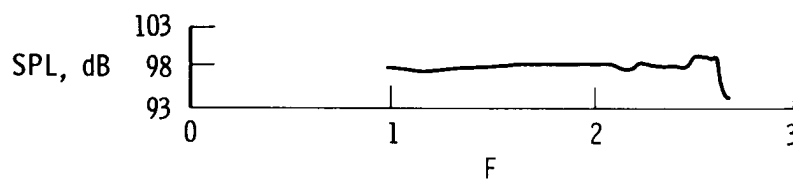
(a) Transducer sensitivity (-55 dB ref. 1 volt/N/m², -35 dB ref. 1 volt/N/m²).



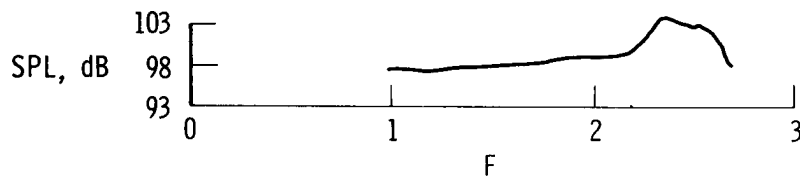
(b) Electrostatic altitude sensitivity response.



(c) Acoustic pressure coupler response.

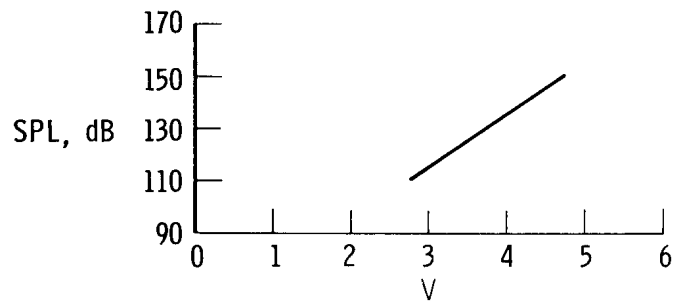


(d) Parallel incidence free field response.

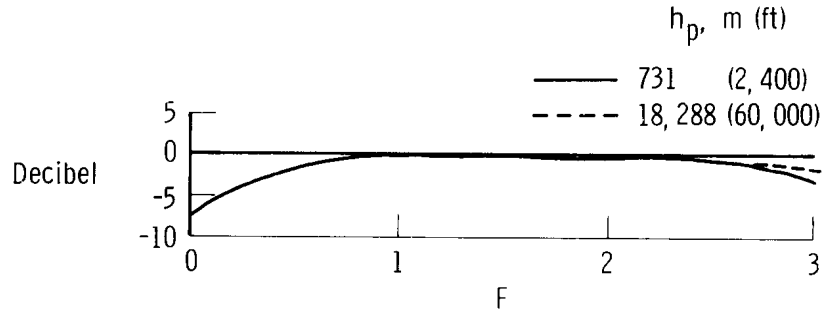


(e) Perpendicular incidence free field response.

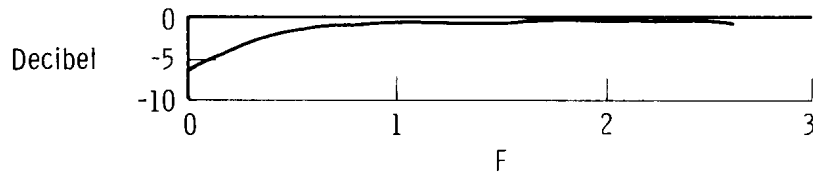
Figure 9. Laboratory calibration for the ES model 299507 microphone (location 6).



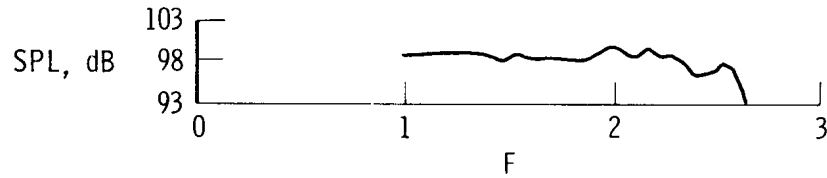
(a) Transducer sensitivity (-63 dB ref. 1 volt/N/m²).



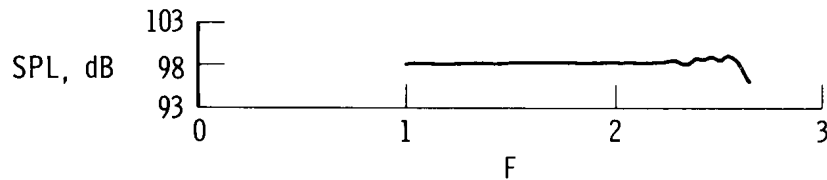
(b) Electrostatic altitude sensitivity response.



(c) Acoustic pressure coupler response.

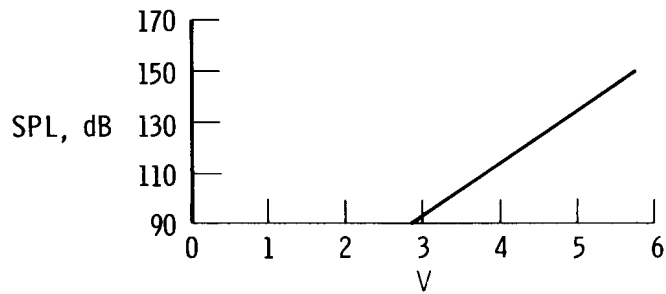


(d) Parallel incidence free field response.

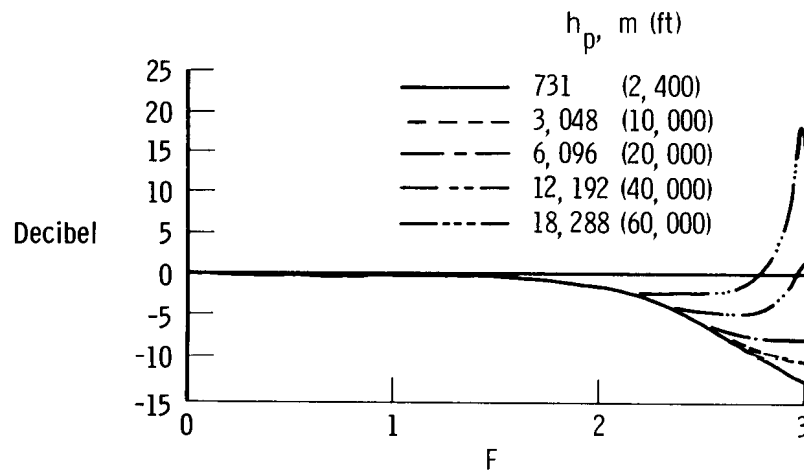


(e) Perpendicular incidence free field response.

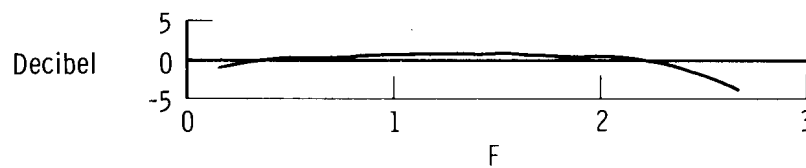
Figure 10. Laboratory calibration for the B & K model 4136 microphone (location 7).



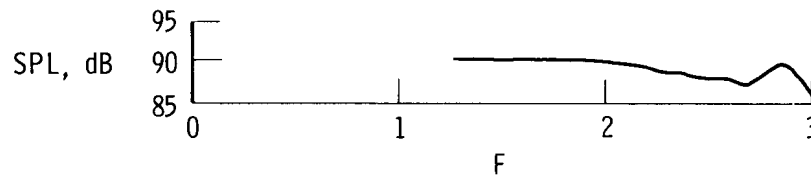
(a) Transducer sensitivity (-40 dB ref. 1 volt/N/m²).



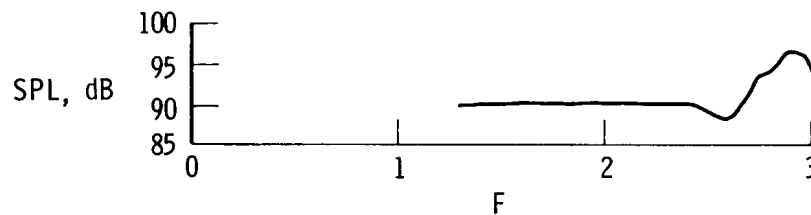
(b) Electrostatic altitude sensitivity response.



(c) Acoustic pressure coupler response.

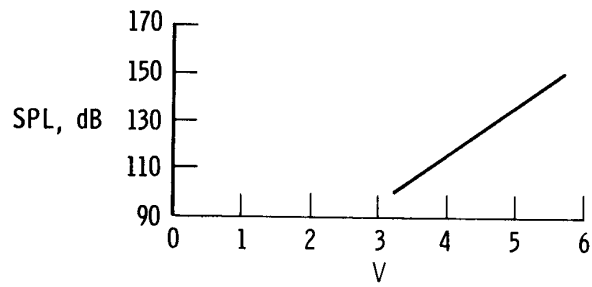


(d) Parallel incidence free field response.

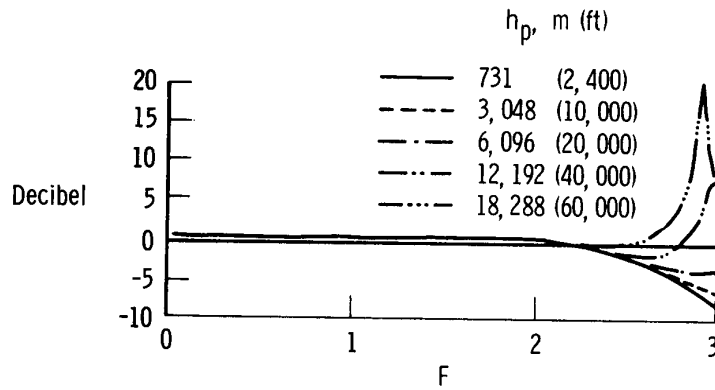


(e) Perpendicular incidence free field response.

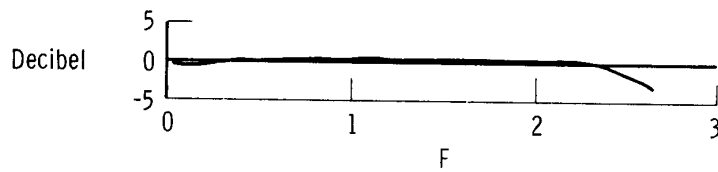
Figure 11. Laboratory calibration for the Photocon model 504, grid-covered microphone (location 8).



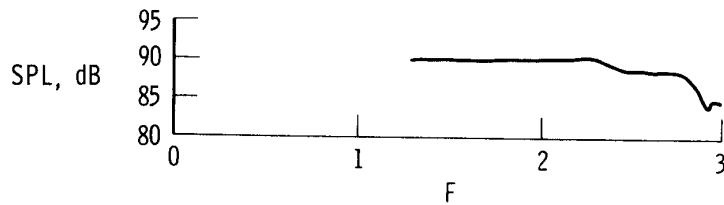
(a) Transducer sensitivity (-42 dB ref. 1 volt/N/m²).



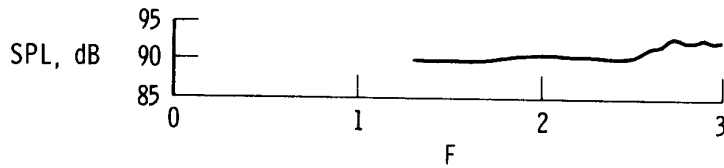
(b) Electrostatic altitude sensitivity response.



(c) Acoustic pressure coupler response.

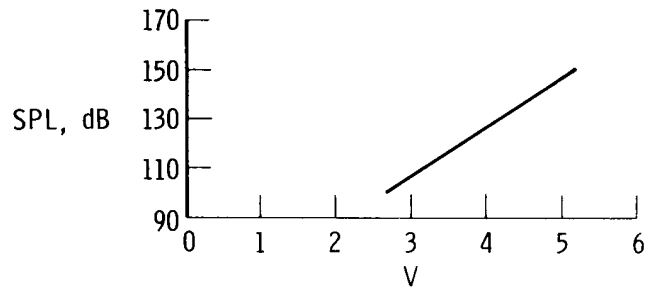


(d) Parallel incidence free field response.

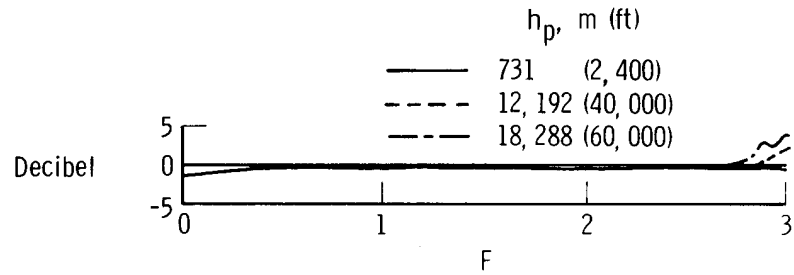


(e) Perpendicular incidence free field response.

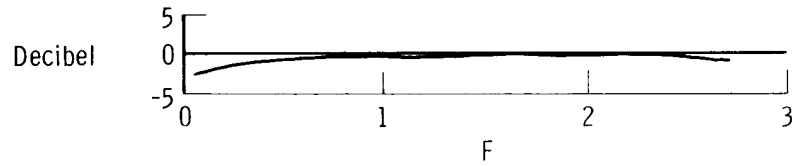
Figure 12. Laboratory calibration for the Photocon model 514 microphone (location 9).



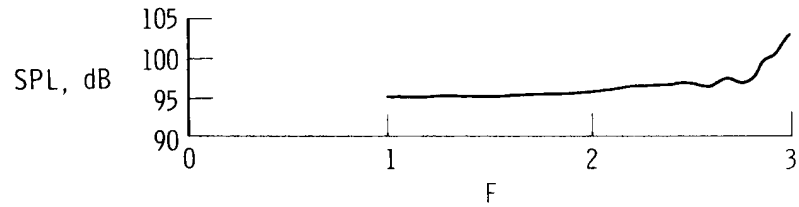
(a) Transducer sensitivity (-52 dB ref. 1 volt/N/m²).



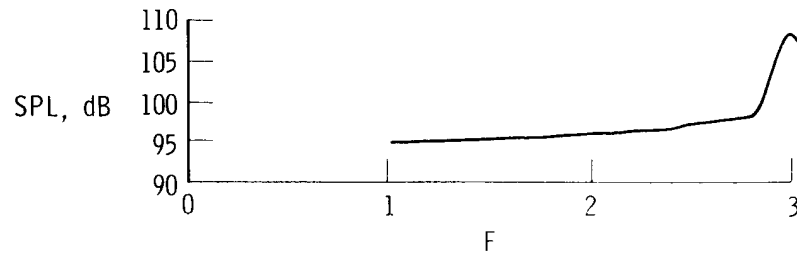
(b) Electrostatic altitude sensitivity response.



(c) Acoustic pressure coupler response.

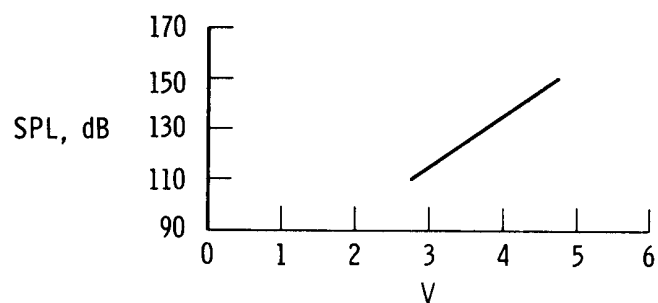


(d) Parallel incidence free field response.

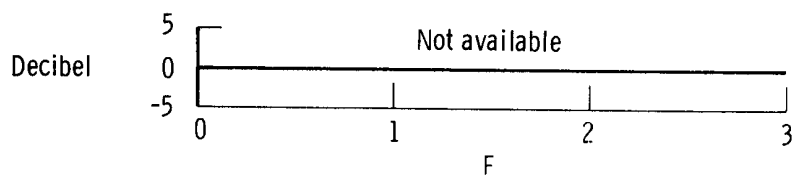


(e) Perpendicular incidence free field response.

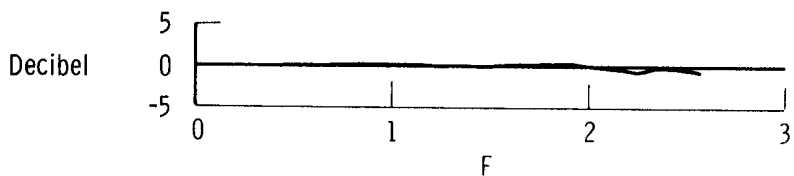
Figure 13. Laboratory calibration for the Photocon model 614 microphone (location 10).



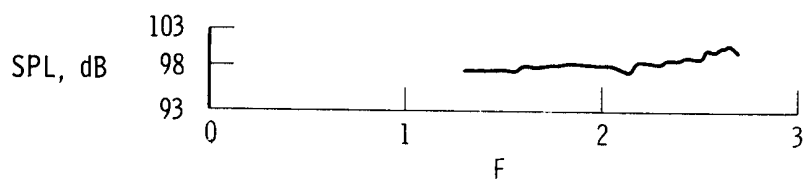
(a) Transducer sensitivity (-62 dB ref. 1 volt/N/m²).



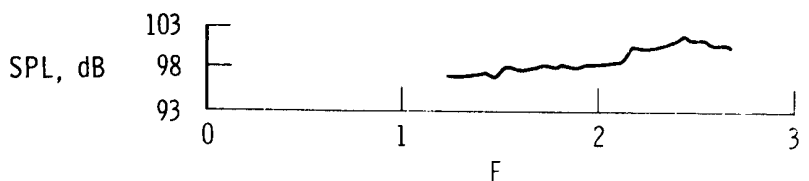
(b) Electrostatic altitude sensitivity response.



(c) Acoustic pressure coupler response.

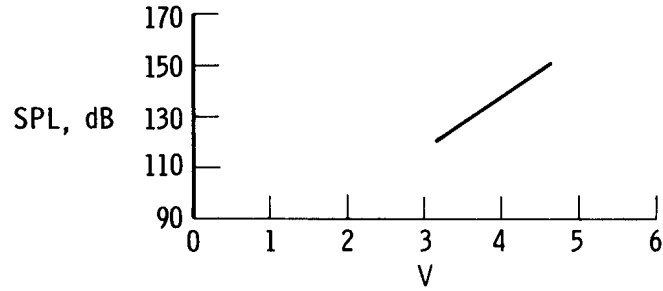


(d) Parallel incidence free field response.

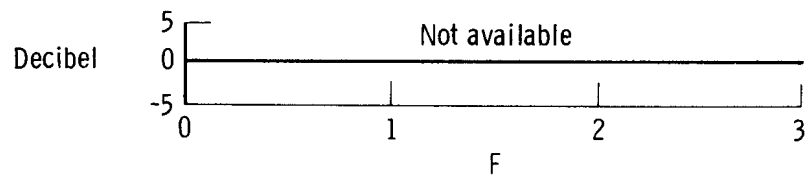


(e) Perpendicular incidence free field response.

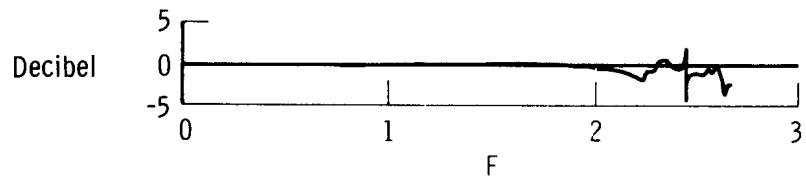
Figure 14. Laboratory calibration for the Kistler model 606L microphone (location 11).



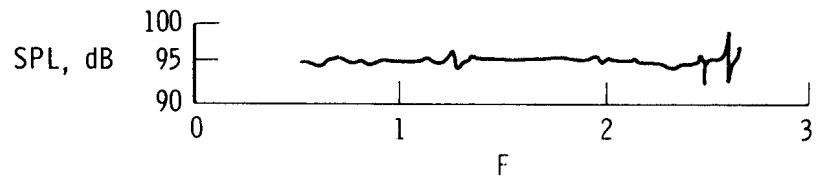
(a) Transducer sensitivity (-63 dB ref. 1 volt/N/m²).



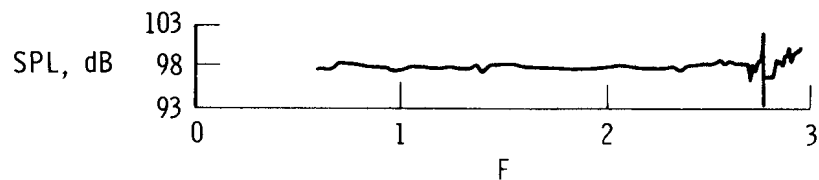
(b) Electrostatic altitude sensitivity response.



(c) Acoustic pressure coupler response.



(d) Parallel incidence free field response.



(e) Perpendicular incidence free field response.

Figure 15. Laboratory calibration for the Kulite model XPL-125-4HF microphone (reference plate).

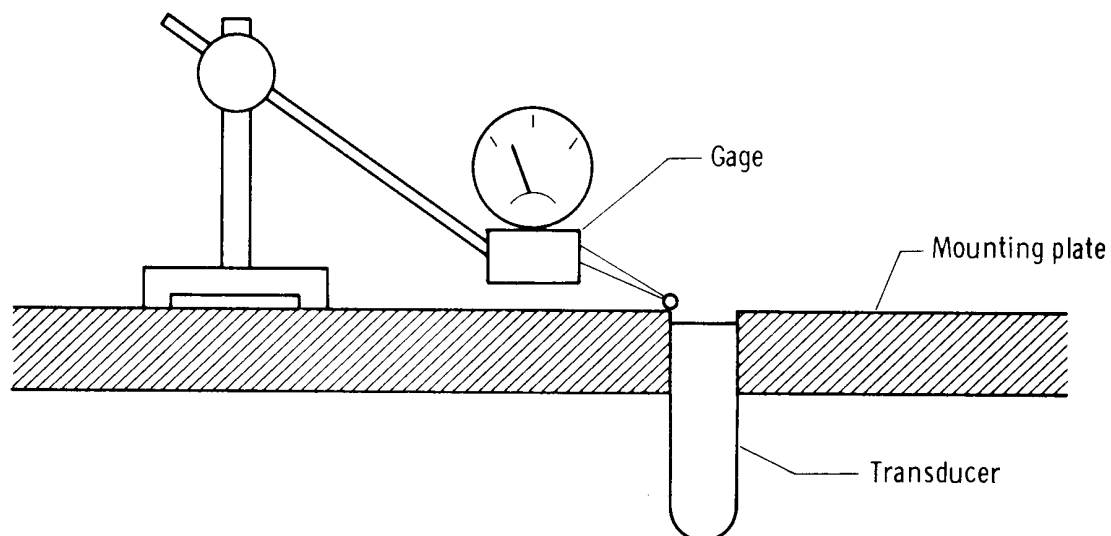


Figure 16. Method of measuring the flushness of the transducers installed in the mounting plates.

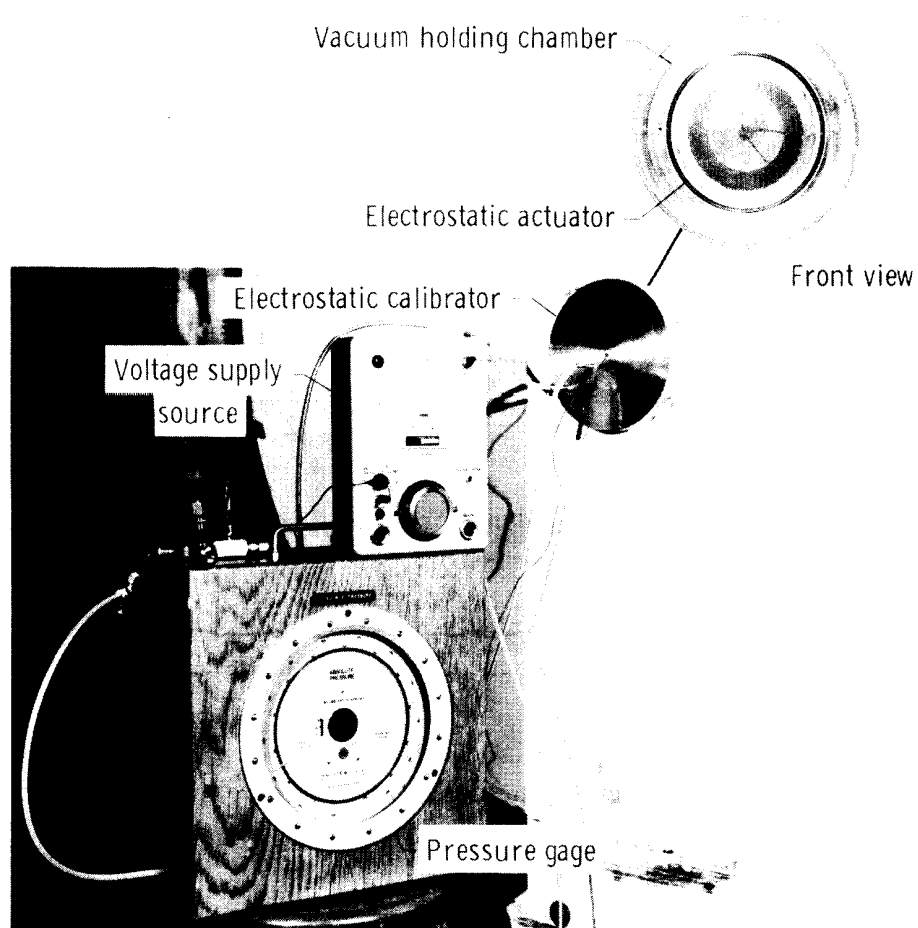


Figure 17. Equipment used to calibrate the installed transducers.

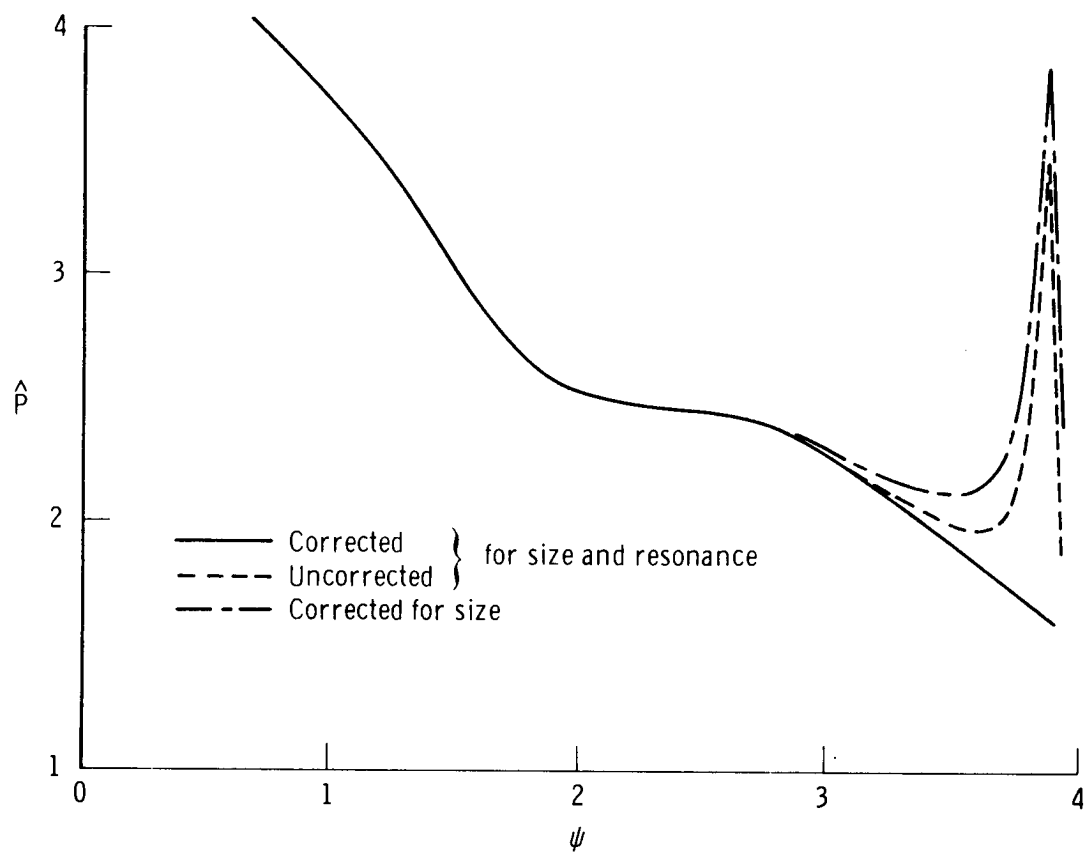


Figure 18. Effect of correction for size and resonance on the estimated power spectral density measured by the Photocon 514 transducer (location 9).

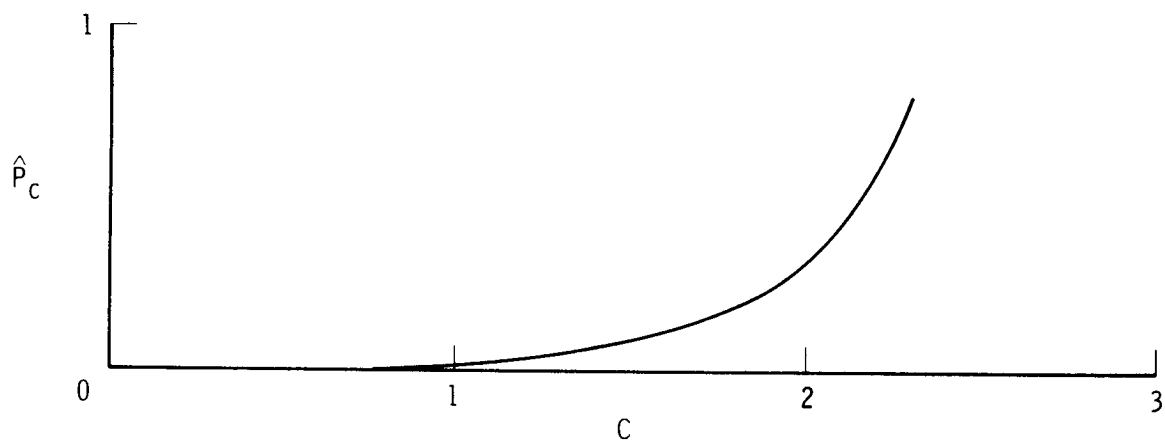


Figure 19. Corcos size correction to estimated power spectral density as a function of a nondimensional frequency parameter.

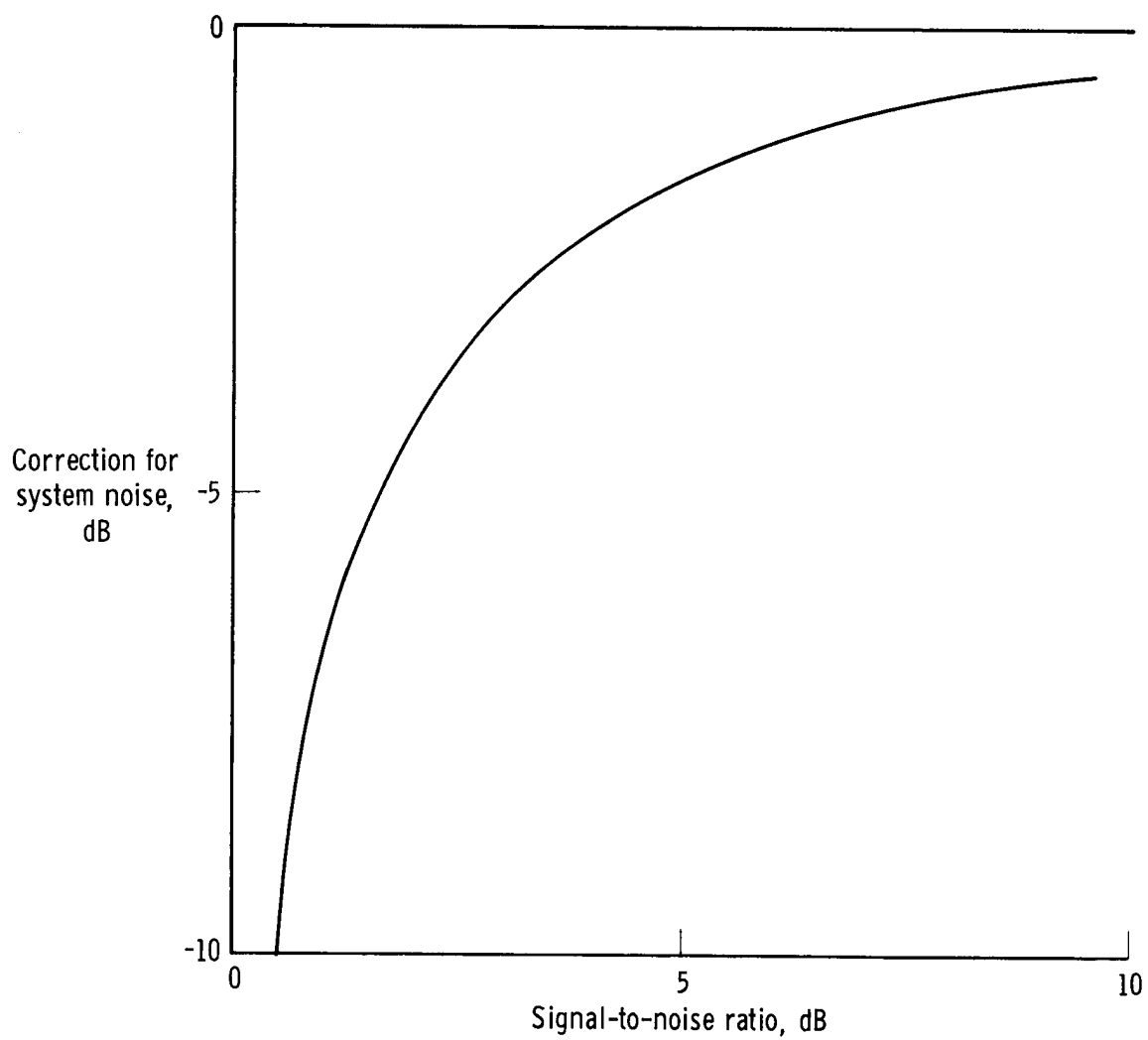
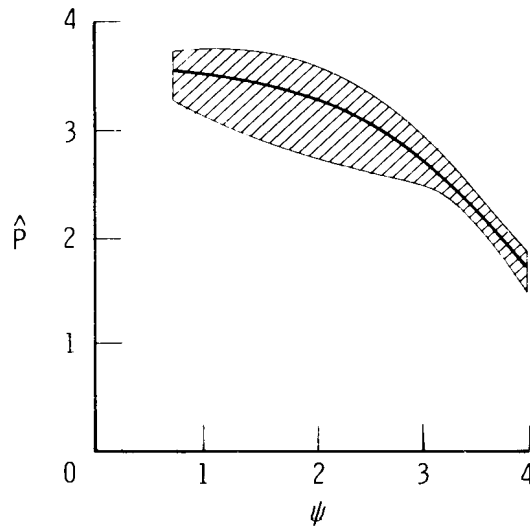
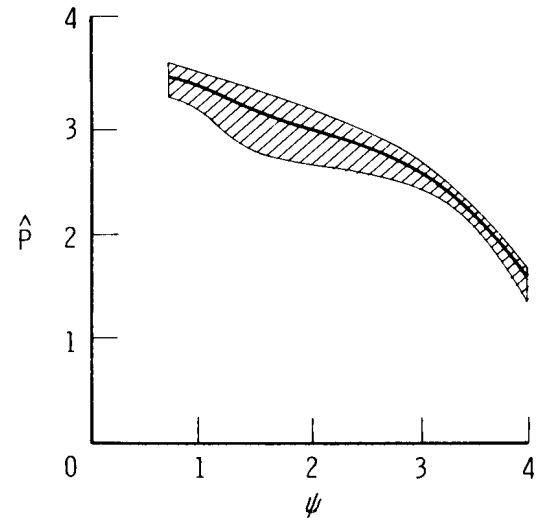


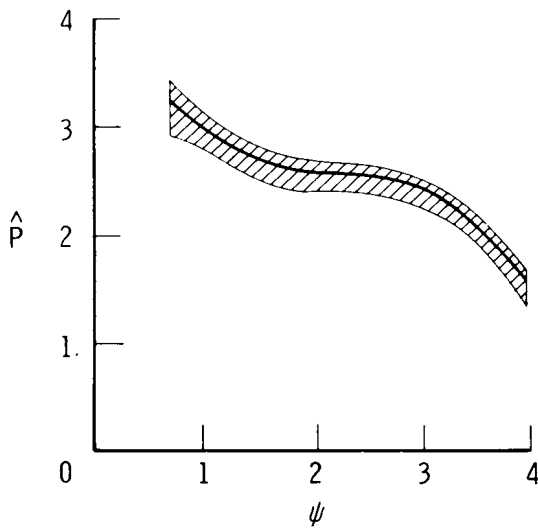
Figure 20. Plot used to determine the correction for system noise.



(a) $M = 1.6$.



(b) $M = 2.0$.



(c) $M = 2.5$.

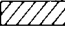

 Data spread for all locations
 Mean pressure spectrum

Figure 21. Variations in the estimated power-spectral-density measurements of the surface-pressure fluctuations determined by data from the reference (Kulite) transducers.

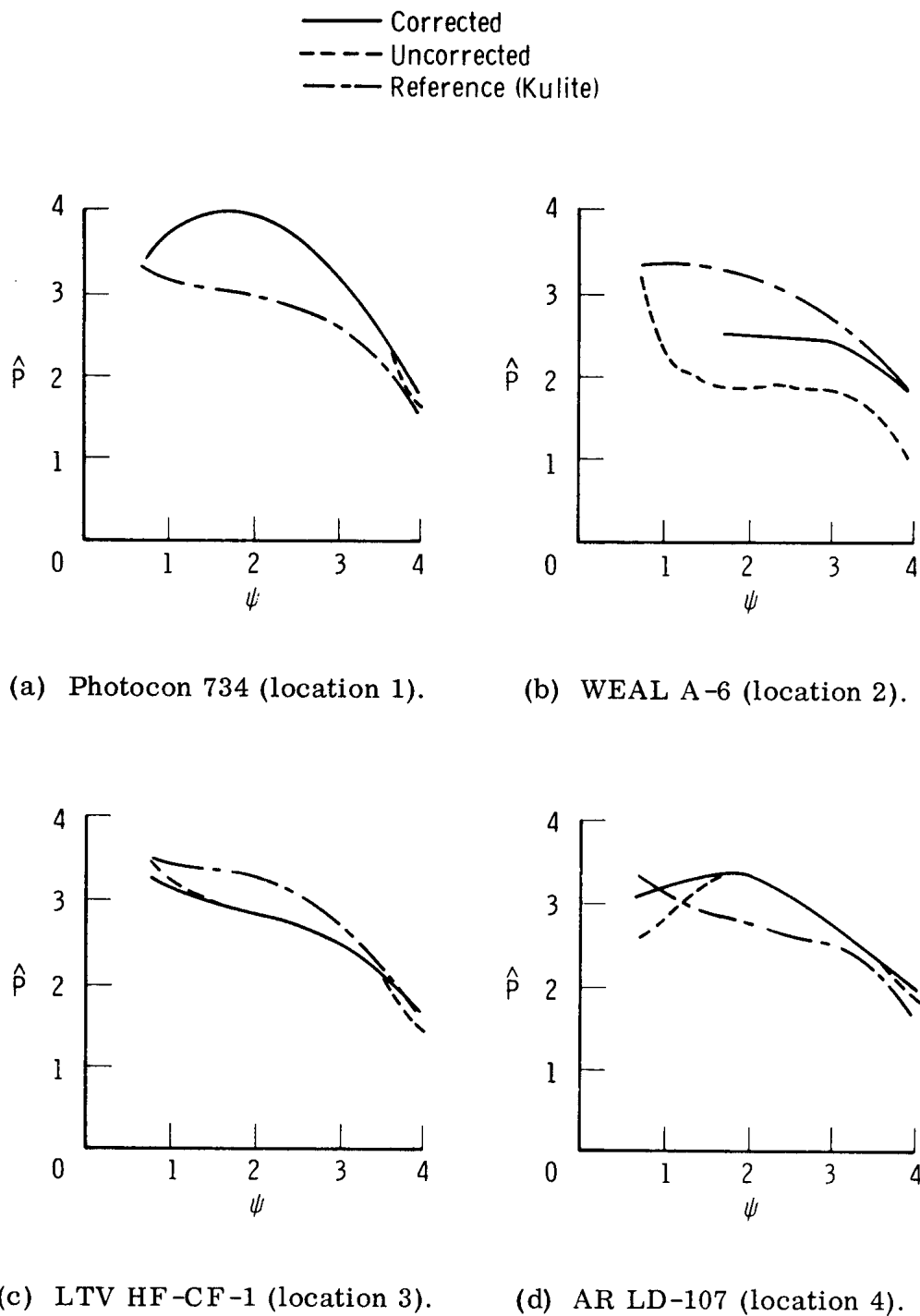
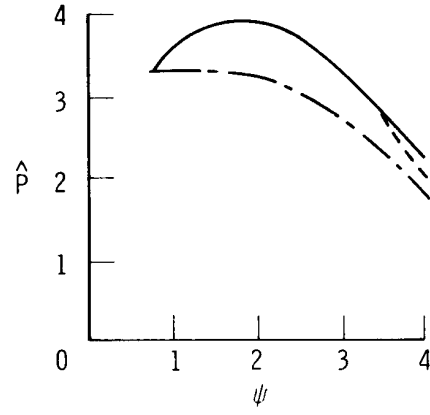
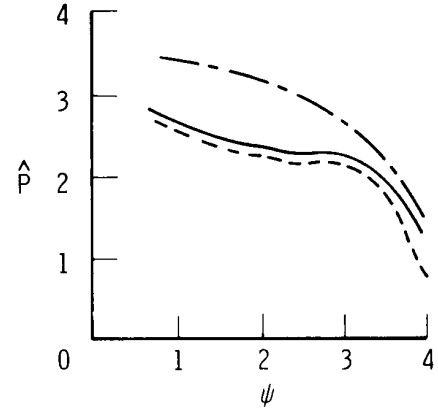


Figure 22. Comparison of measurements of estimated power spectral density from 11 different transducers with measurements from reference (Kulite) transducers. $M = 1.6$.

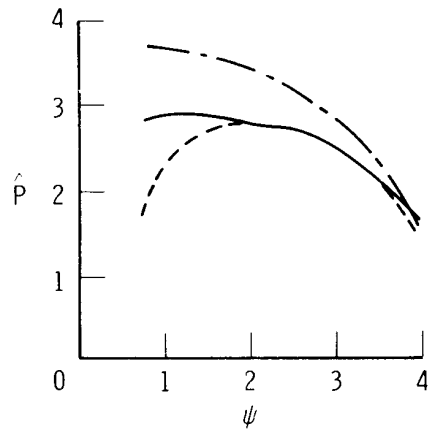
— Corrected
 - - - Uncorrected
 - - - Reference (Kulite)



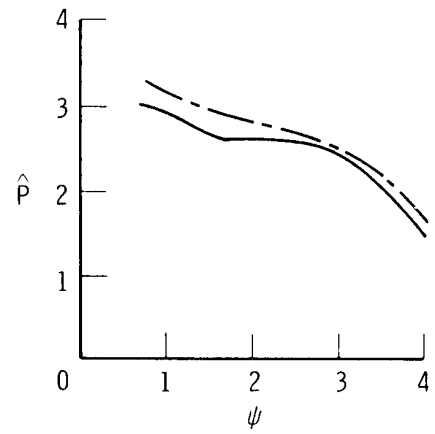
(e) BBN 376A (location 5).



(f) ES 299507 (location 6).



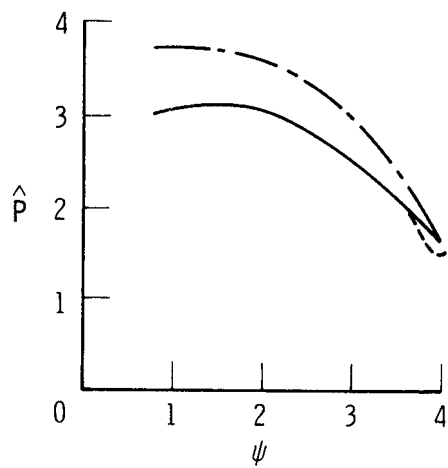
(g) B & K 4136 (location 7).



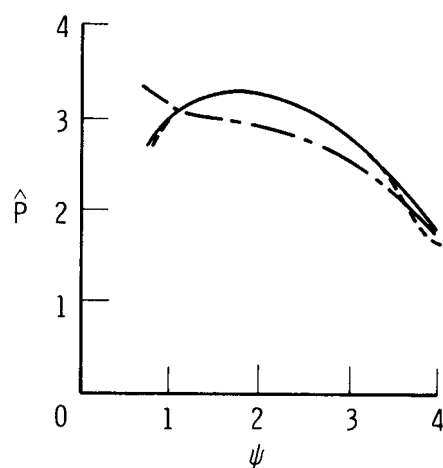
(h) Photocon 504 (location 8).

Figure 22. Continued.

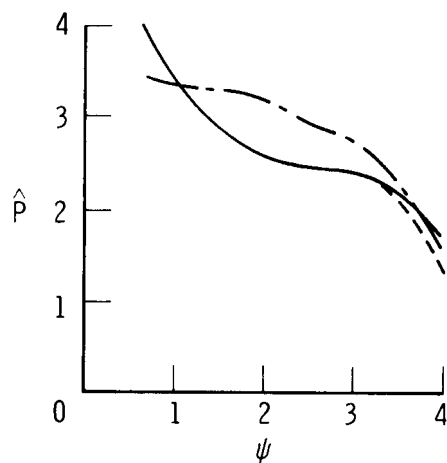
— Corrected
 - - - Uncorrected
 - · - Reference (Kulite)



(i) Photocon 514 (location 9).



(j) Photocon 614 (location 10).



(k) Kistler 606 L (location 11).

Figure 22. Concluded.

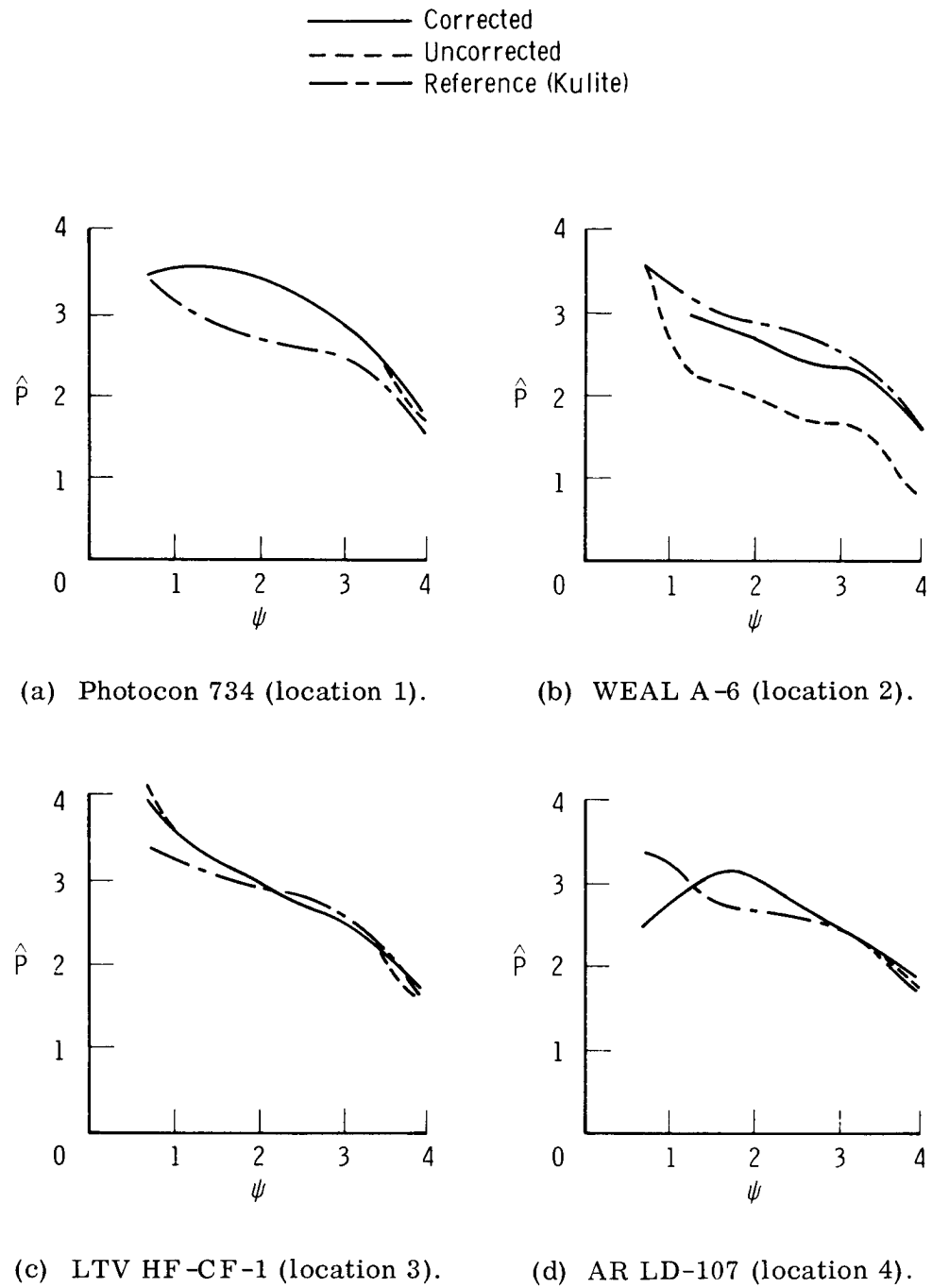
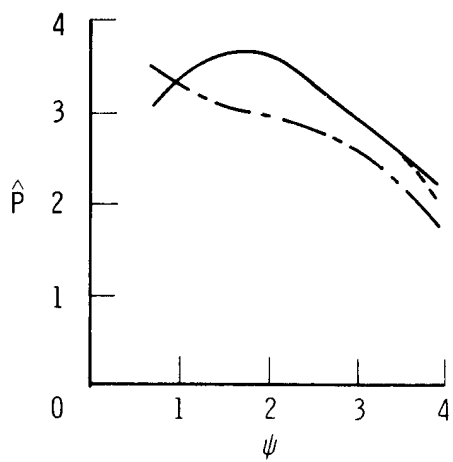
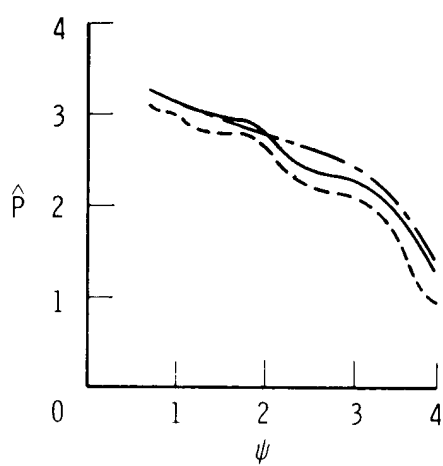


Figure 23. Comparison of measurements of estimated power spectral density from 11 different transducers with measurements from reference (Kulite) transducers. $M = 2.0$.

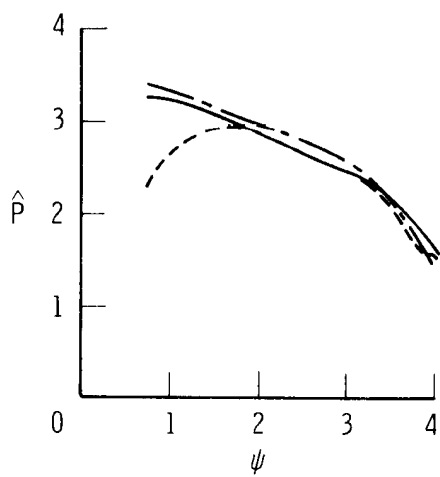
— Corrected
 - - - Uncorrected
 - · - Reference (Kulite)



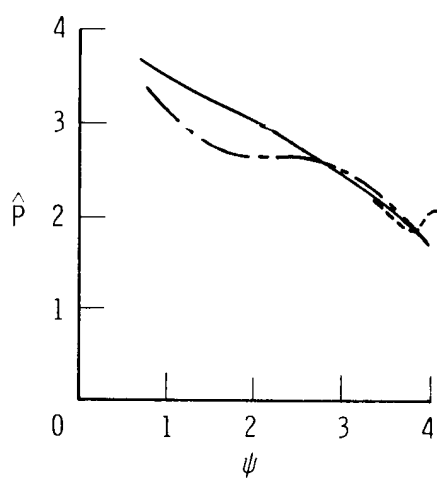
(e) BBN 376A (location 5).



(f) ES 299507 (location 6).

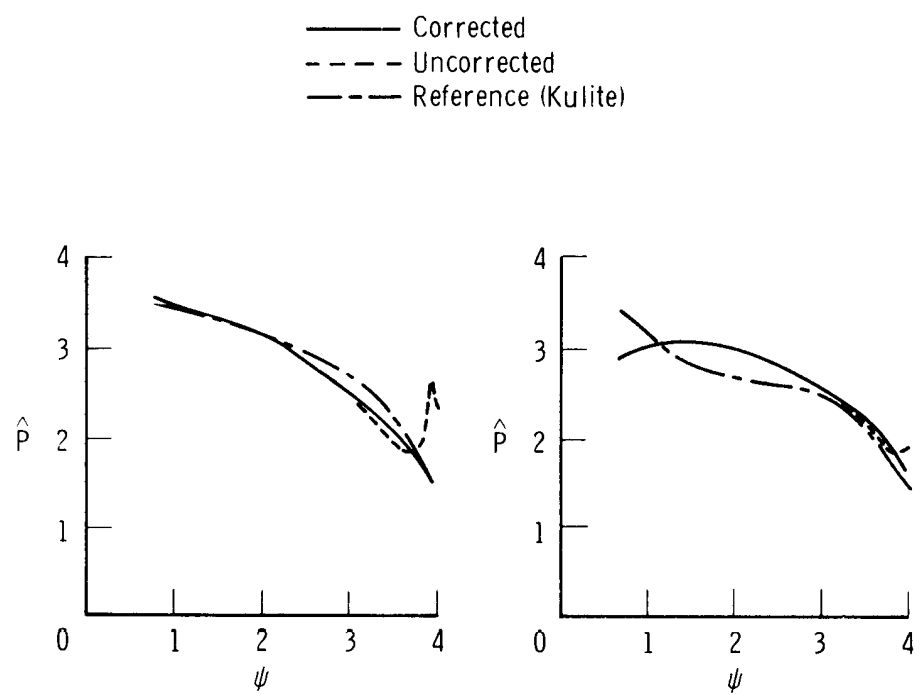


(g) B & K 4136 (location 7).

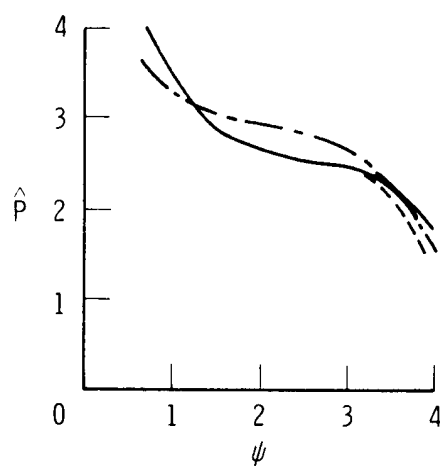


(h) Photocon 504 (location 8).

Figure 23. Continued.



(i) Photocon 514 (location 9). (j) Photocon 614 (location 10).



(k) Kistler 606L (location 11).

Figure 23. Concluded.

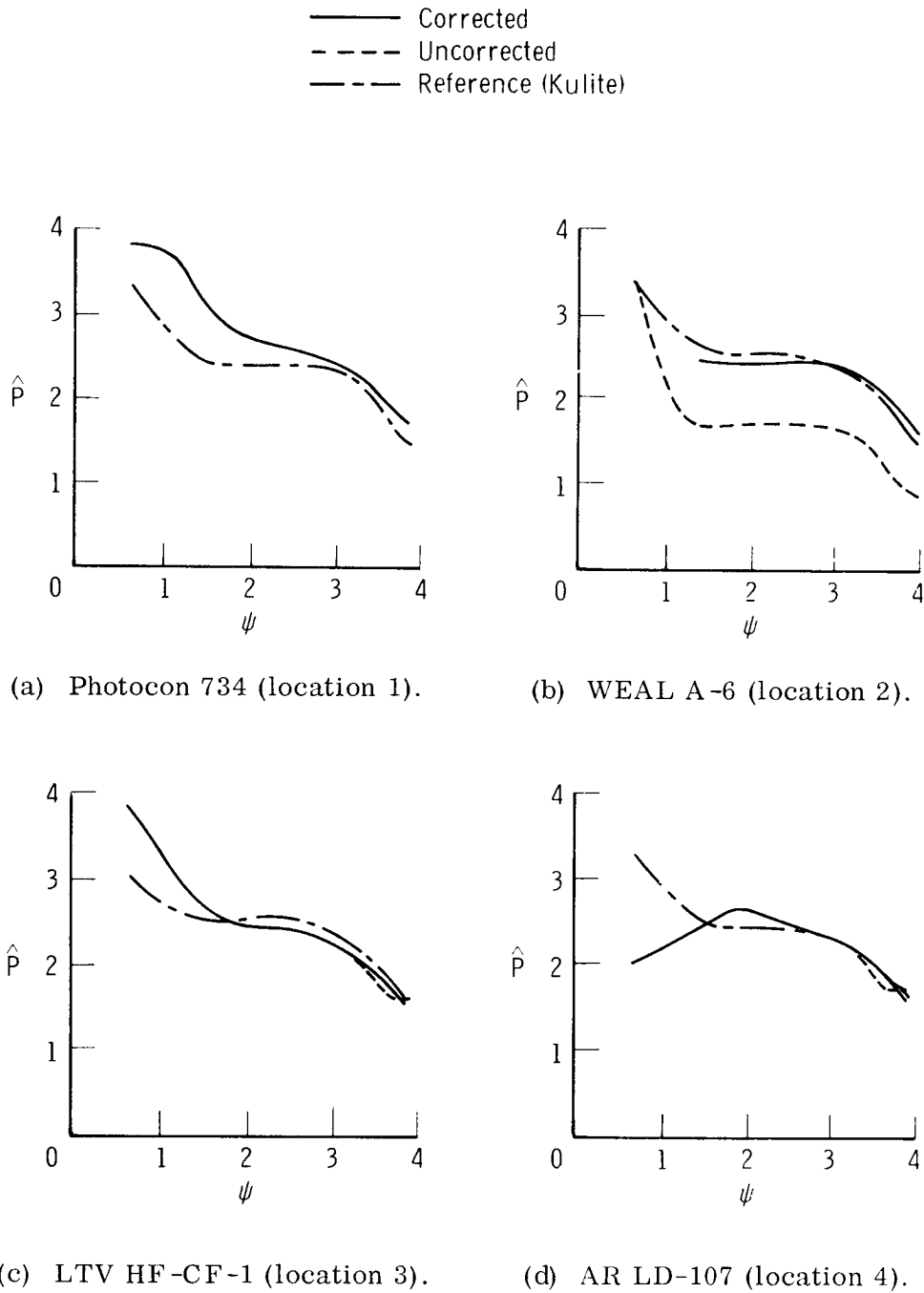
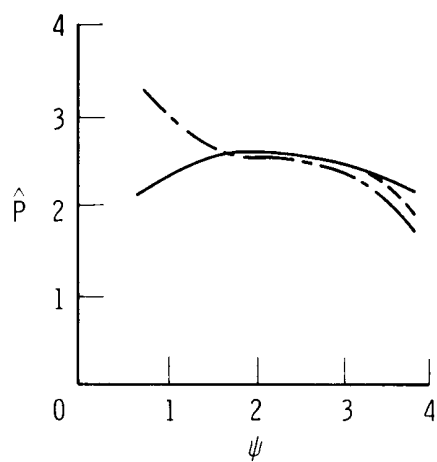
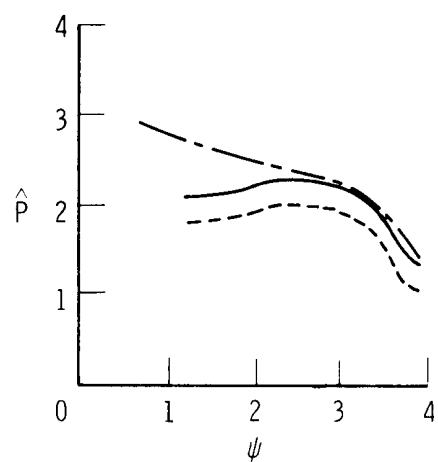


Figure 24. Comparison of measurements of estimated power spectral density from 11 different transducers with measurements from reference (Kulite) transducers. $M = 2.5$.

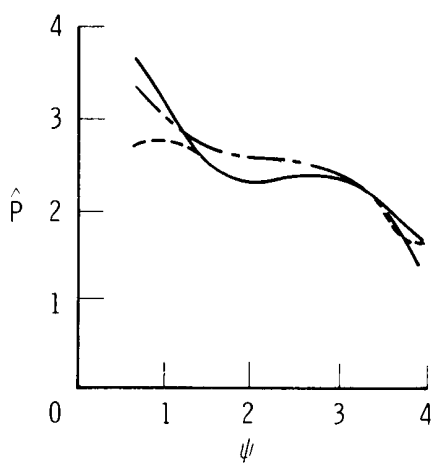
— Corrected
 - - - Uncorrected
 - · - Reference (Kulite)



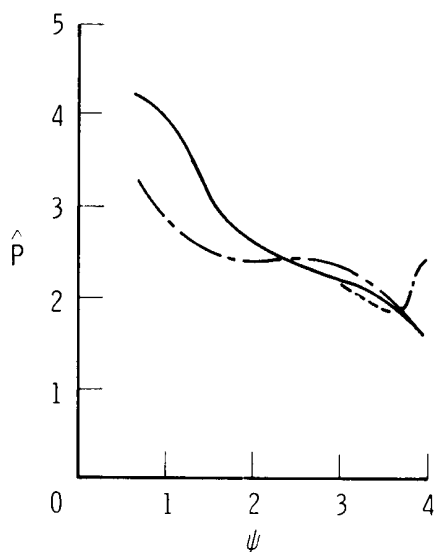
(e) BBN 376A (location 5).



(f) ES 299507 (location 6).



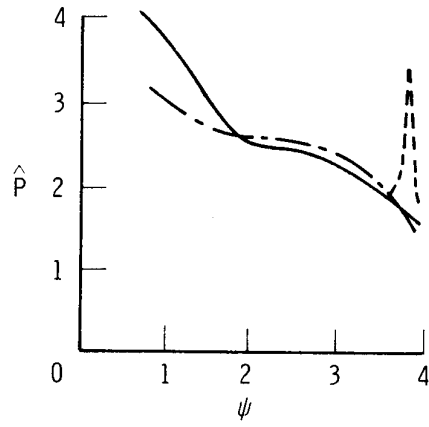
(g) B & K 4136 (location 7).



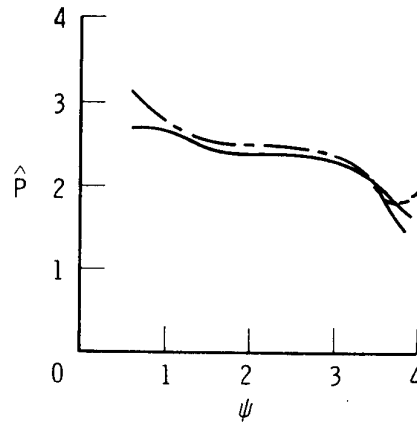
(h) Photocon 504 (location 8).

Figure 24. Continued.

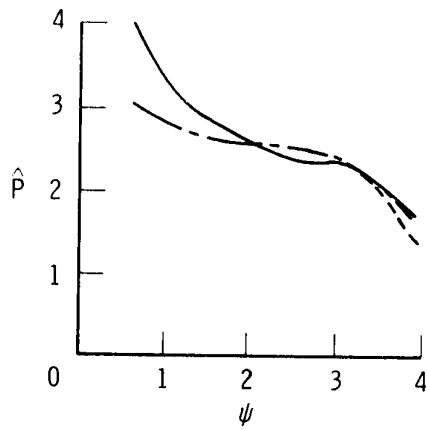
— Corrected
 - - - Uncorrected
 - - - Reference (Kulite)



(i) Photocon 514 (location 9).

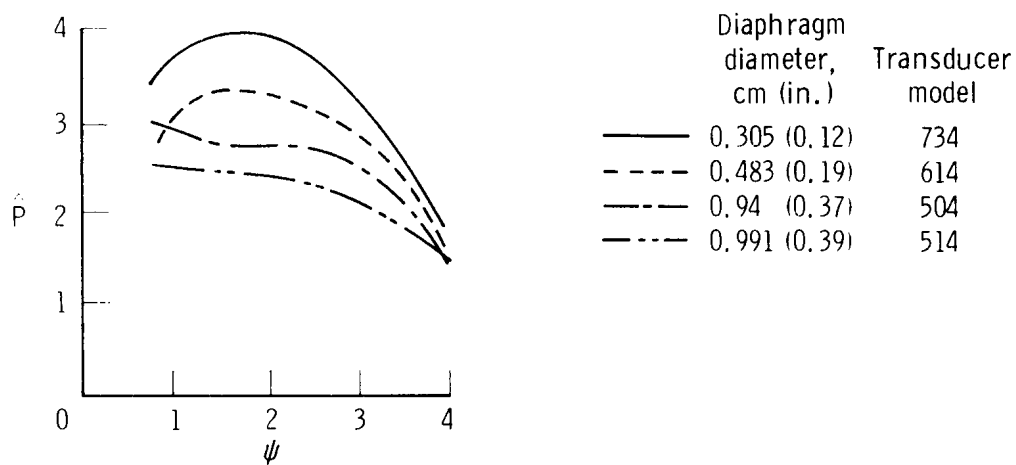


(j) Photocon 614 (location 10).

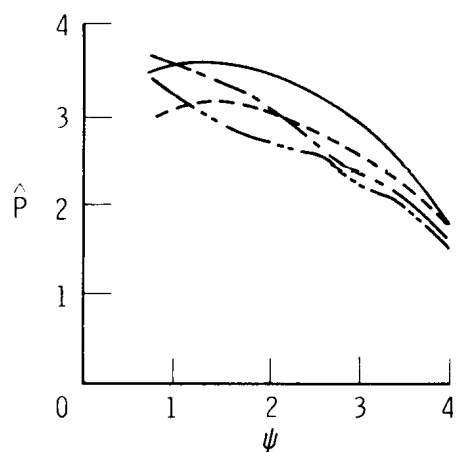


(k) Kistler 606L (location 11).

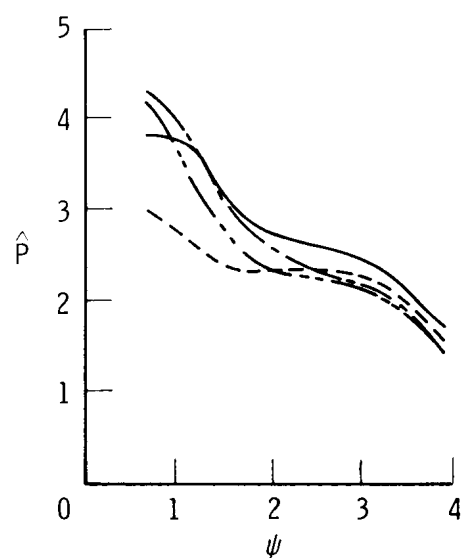
Figure 24. Concluded.



(a) $M = 1.6$.

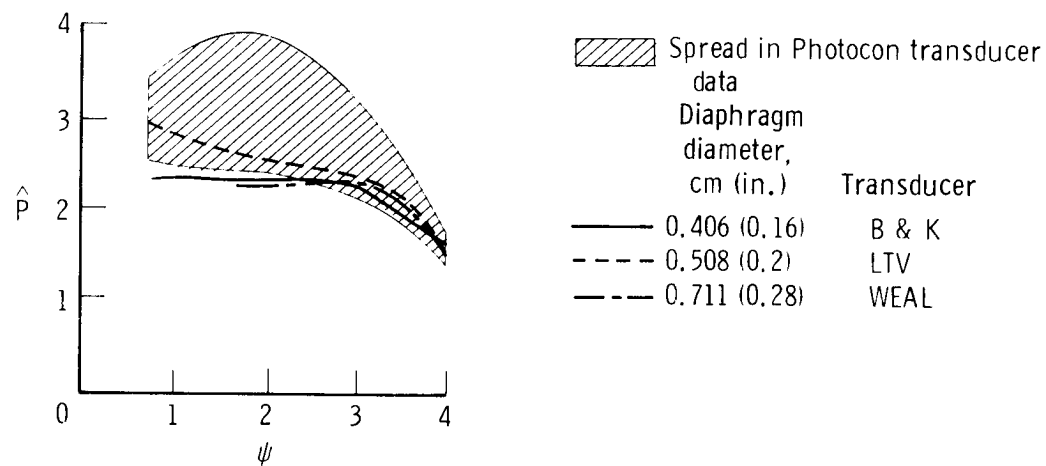


(b) $M = 2.0$.

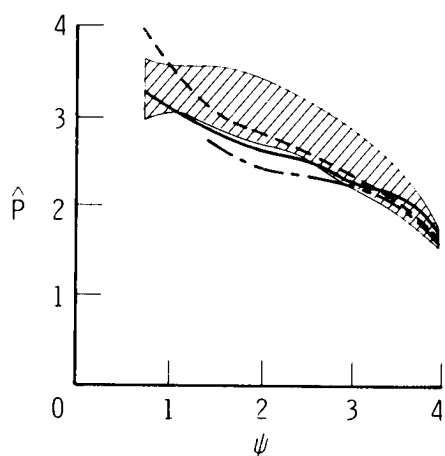


(c) $M = 2.5$.

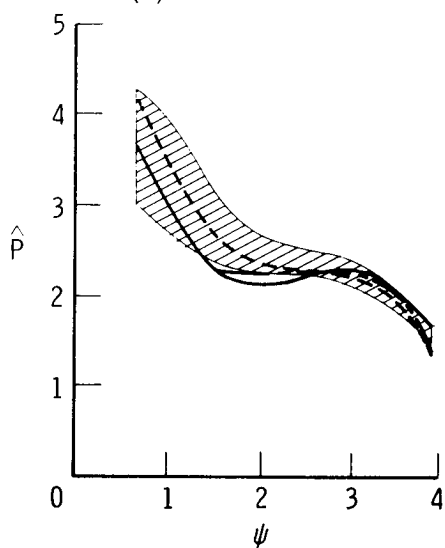
Figure 25. Comparison of the estimated power-spectral-density measurements from the Photocon transducers. Data corrected to location 1.



(a) $M = 1.6$.

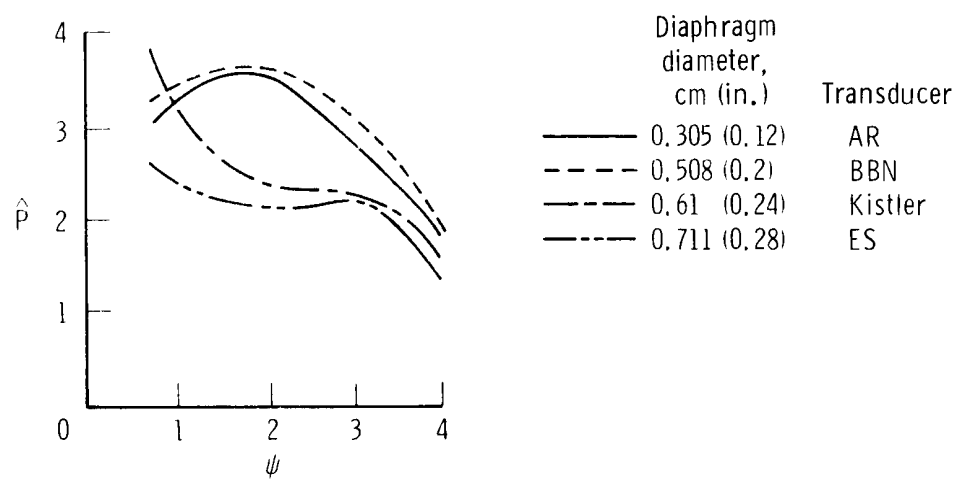


(b) $M = 2.0$.

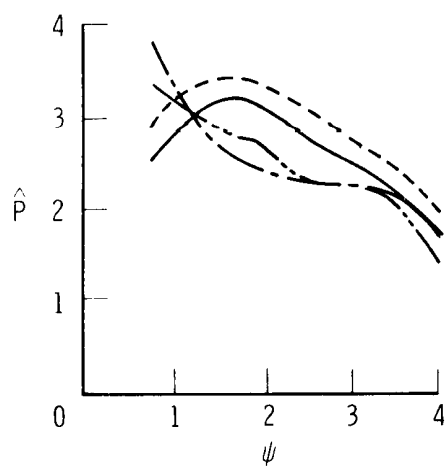


(c) $M = 2.5$.

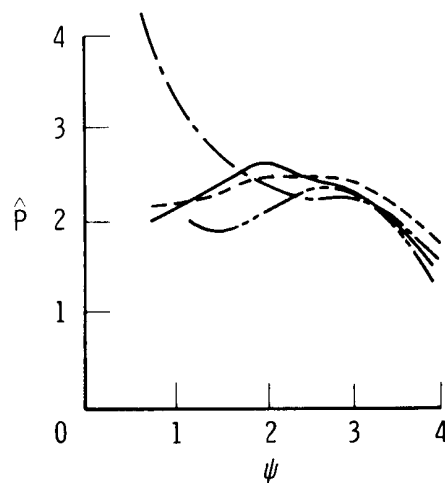
Figure 26. Comparison of the estimated power-spectral-density measurements from the WEAL, LTV, B & K, and Photocon transducers. Data corrected to location 1.



(a) $M = 1.6$.



(b) $M = 2.0$.



(c) $M = 2.5$.

Figure 27. Comparison of the estimated power-spectral-density measurements from the AR, BBN, Kistler, and ES transducers. Data corrected to location 1.

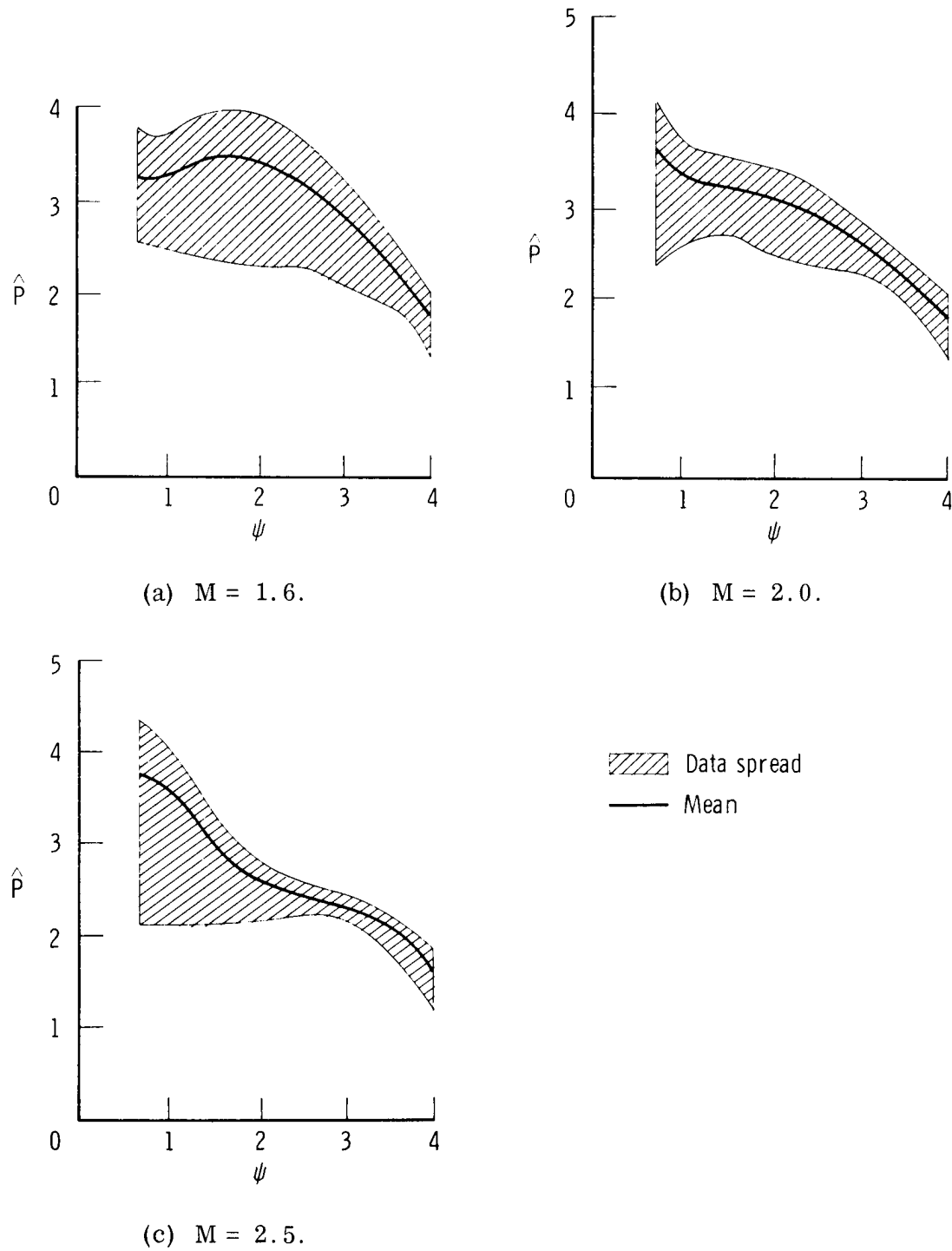


Figure 28. Variations in the estimated power-spectral-density measurements of the surface-pressure fluctuations as determined from the 11 different transducers. Data corrected to location 1.

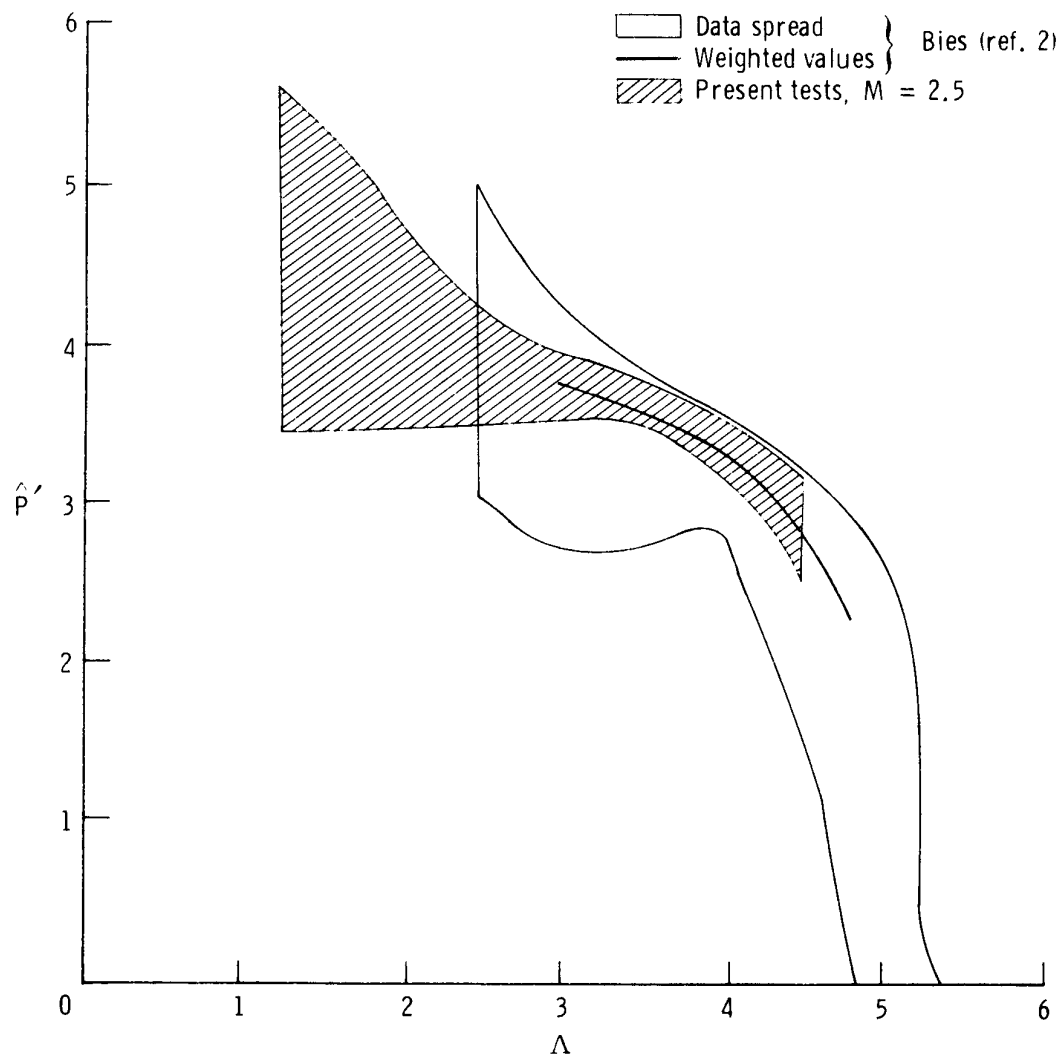


Figure 29. Comparison of the variation in the estimated power-spectral-density measurements at $M = 2.5$ with results from reference 2.